Geologic Nozzles[1]

Susan Werner Kieffer
U.S. Geological Survey, Flagstaff, Arizona 86001

Abstract

Sonic velocities of geologic fluids, such as volcanic magmas and geothermal fluids, can be as low as 1 m/s. Critical velocities in large rivers can be of the order of 1-10 m/s. Because velocities of fluids moving in these settings can exceed these characteristic velocities, sonic and supersonic gas flow and critical and supercritical shallow-water flow can occur. The importance of the low characteristic velocities of geologic fluids has not been widely recognized and, as a result, the importance of supercritical and supersonic flow in geological processes has generally been underestimated. The lateral blast at Mount St. Helens, Washington, propelled a gas heavily laden with dust into the atmosphere. Because of the low sound speed in this gas (about 100 m/s), the flow was internally supersonic. Old Faithful Geyser, Wyoming, is a converging-diverging nozzle in which liquid water refilling the conduit during the recharge cycle changes during eruption into a two-phase liquid-vapor mixture with a very low sound velocity. The high sound speed of liquid water determines the characteristics of harmonic tremor observed at the geyser during the recharge interval, whereas the low sound speed of the liquid-vapor mixture influences the fluid-flow characteristics of the eruption. At the rapids of the Colorado River in the Grand Canyon, Arizona, supercritical flow occurs where debris discharged from tributary canyons constricts the channel into the shape of a converging-diverging nozzle. The geometry of the channel in these regions can be used to interpret the flood history of the Colorado River over the past 10^3-10^5 years. The unity of fluid mechanics in these three natural phenomena is provided by the well-known analogy between gas flow and shallow-water flow in converging-diverging nozzles.

I. Introduction: geologic nozzles

An eruption of Old Faithful geyser, a flood on the Colorado River, and a lateral blast from Mount St. Helens do not, at first glance, appear to be related. A geographic map of the locations of these three places certainly does not reveal any underlying geologic unity (Fig. 1). However, a fluid-dynamical unity is revealed when the "locations" are shown instead on a schematic diagram[2] of gas flowing through a nozzle or shallow water flowing through a flume (Fig. 2). The analogy between the flow fields for compressible gas and shallow water is semiquantitative and was thus widely explored in the early days of wind-tunnel development[3]. In modern times the analogy has been

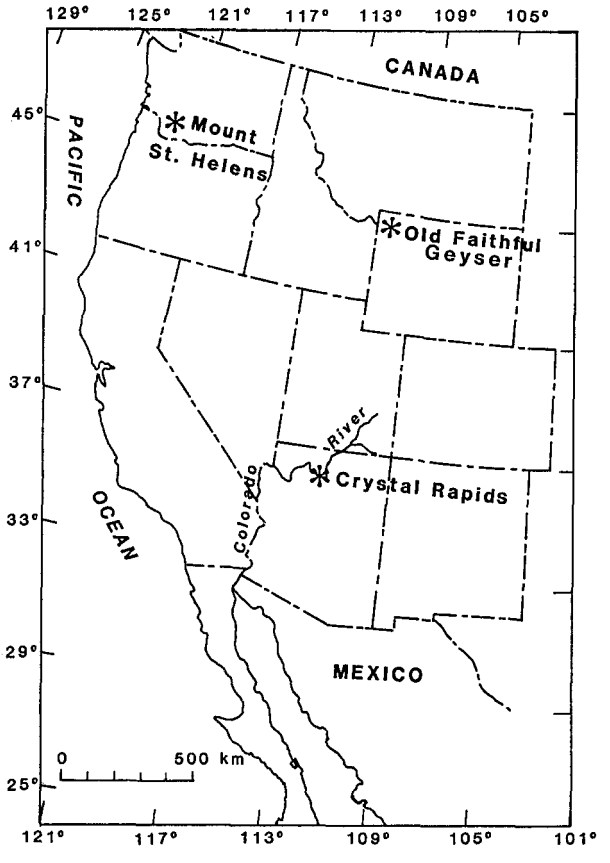

FIG. 1. Index map of the geographic locations of Crystal Rapids (Grand Canyon, Arizona), Old Faithful Geyser (Yellowstone National Park, Wyoming), and Mount St. Helens (Washington).

primarily a teaching tool[4] and has never been used by geologists to explain large-scale natural phenomena. The purpose of this paper is to show the basis for invoking nozzle-flow theory for interpretation of complex geologic events and to provide a perspective on geological problems in which the importance of supercritical and supersonic flow has been underestimated.

A major reason that geologic events have not been viewed from the particular perspective of fluid mechanics presented here is the subdivision of fluid mechanics and its applied fields into the specialties of compressible and incompressible flow; for example, aeronautics versus hydraulics. This subdivision arises from the need to simplify the complex momentum and continuity equations in order to solve practical problems. The momentum equation for a viscous fluid moving in a gravitational field under the influence of a pressure gradient is complex because of dimensionality and nonlinearity:

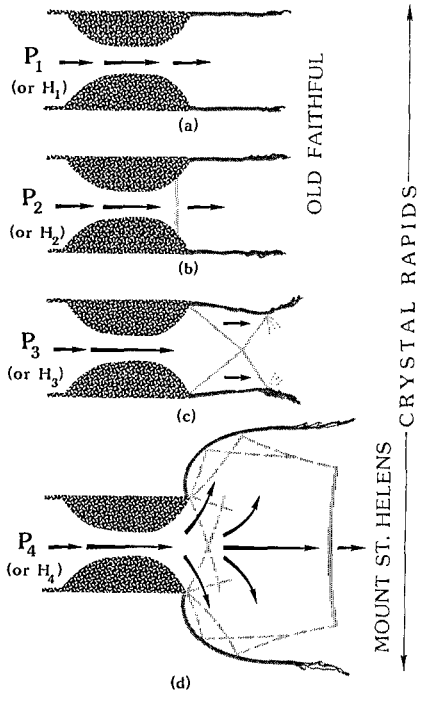

FIG. 2. Four diagrams showing the behavior of gas flowing through a converging-diverging nozzle, or of shallow water flowing through a converging-diverging flume; arranged vertically. The nozzle walls are shown by the heavy lines and heavy shading at the left; the flow direction is indicated by arrows, and the velocity magnitude is indicated schematically by the length of the arrows. The reservoir of gas or liquid is on the left: $P_1, P_2, \ldots$ represent increasingly larger reservoir pressures, and H_1, $H_2, \ldots$ represent increasingly larger values of hydraulic head, compared to ambient or downstream conditions on the right. At the exit of the nozzle (or channel) on the right, the structure of the flow field in the departing fluid is shown schematically by medium shading. Shock and rarefaction waves (alternatively, positive and negative normal and oblique hydraulic jumps) are indicated by the lightest shading. Relative flow conditions are shown schematically by the position of the lettering at the right: Old Faithful is subsonic (a) or weakly supersonic (b), Mount St. Helens is strongly supersonic (d), and Crystal Rapids involves all conditions (a-d) from subcritical to strongly supercritical.

$$\rho \frac{D\mathbf{u}}{Dt} = -\nabla P + \nabla \cdot \tau + \rho \mathbf{g} \ . \tag{1}$$

In this equation, ρ is the fluid density, D/Dt is the material derivative, $\mathbf{u}$ is the fluid velocity, ∇P is the pressure force acting on the fluid, $\nabla \cdot \tau$ is the viscous force, and $\mathbf{g}$ is the acceleration of gravity. The continuity equation for mass is generally simpler, but is still difficult to apply in a geometrically complicated problem:

$$\frac{D\rho}{Dt} = -\rho(\nabla \cdot \mathbf{u}) \ . \tag{2}$$

In many cases these two important equations can be considerably simplified by consideration of the fluid properties or the boundary conditions of the problem. For example, if pressure changes are relatively small, compressibility can be neglected, so that $\rho \sim$ constant and $\nabla \cdot \mathbf{u} = 0$. Such an assumption underlies all of hydraulics, and geologists with interests in hydraulics or related geomorphic problems typically diverge at an early stage of their education from advanced studies of compressible fluid dynamics.

Alternatively, in many flows the pressure gradient may be great enough so that compressibility is important but gravity is not; $\mathbf{g} \sim 0$. This latter condition is assumed in most of gas dynamics and, because of the prominent role of gravity in most geologic processes, few geologists are exposed to a rigorous gas-dynamics curriculum.

Although the subjects of nozzle gas dynamics and of shallow-water hydraulics evolve from very different approximations to the conservation equations, important concepts common to both subjects have been recognized because, when reduced to suitable nondimensional variables, the conservation equations in the two subjects become identical. (Readers familiar with this identity can skip directly to Section II.)

Examine first the mass and momentum equations for a perfect gas. For simplicity, assume that the flow is quasi-one-dimensional along a coordinate direction x. The equations of mass and momentum conservation for flow of a compressible gas are

$$\frac{\partial \rho}{\partial t} + u\frac{\partial \rho}{\partial x} + \rho\frac{\partial u}{\partial x} = 0 \tag{3}$$

and

$$\frac{\partial u}{\partial t} + u\frac{\partial u}{\partial x} + \frac{1}{\rho}\frac{\partial P}{\partial x} = 0 \ . \tag{4}$$

For a perfect gas and isentropic flow,

$$P\,V = R\,T \tag{5}$$

and

$$P\,V^{\gamma} = P_o V_o^{\gamma} = \text{constant} \ , \tag{6}$$

where P is pressure, V is volume, R is the gas constant, T is temperature, and γ is the ratio of specific heats (the isentropic exponent). The subscript o indicates a reference state (typically one where the fluid is at rest with velocity $u = u_o = 0$). For a perfect gas, Eqs. (3)-(6) can be combined to give

$$\frac{\partial u}{\partial t} + u\,\frac{\partial u}{\partial x} + \frac{\gamma P_o}{\rho_o^{\gamma}}\,\rho^{\gamma-2}\,\frac{\partial \rho}{\partial x} = 0\,. \tag{7}$$

For water flowing from one infinite reservoir into another with lower head, the equations of motion that can be directly compared with Eqs. (3) and (7) are

$$\frac{\partial h}{\partial t} + u\,\frac{\partial h}{\partial x} + h\,\frac{\partial u}{\partial x} = 0 \tag{8}$$

and

$$\frac{\partial u}{\partial t} + u\,\frac{\partial u}{\partial x} + g\,\frac{\partial h}{\partial x} = 0\,, \tag{9}$$

where h is the water depth. In these equations, and in the figures in this paper, it is assumed that in a vertical cross section (containing the coordinate z), the bottom of the water is at the channel boundary, $z = 0$, and the water has a free surface at $z = h$. The free surface is assumed to be at constant atmospheric pressure, P_a, but its elevation can vary along the channel and with time. The velocity of the water can also vary with position along the channel, but is assumed constant over any vertical cross section. The viscosity and compressibility of the water are ignored. Again, as with gas flow, quasi-one-dimensional flow is assumed -- the contours of the channel walls must be gradual, and vertical accelerations of the water must be small compared with the acceleration of gravity, g.

The shallow-water conservation equations (8) and (9) are identical to the compressible-gas conservation equations (3) and (7) *if* (1) water depth, h, is analogous to gas density, ρ, and (2) the isentropic exponent, γ, of the gas is equal to 2 (a value which, unfortunately, is never attained in real gases, so that the mathematically equivalent flow fields cannot be physically realized). Examination of the conservation equations and the equations of state for a perfect gas shows that h is also analogous to T, and h^2 is analogous to P. Hence, within the context of all of the simplifying assumptions, flow of gas in a nozzle and flow of shallow water in a flume are governed by the same conservation equations. Identical flow fields therefore occur when the proper nondimensional variables are considered.

The illustrations in Fig. 2 represent the flow conditions at different ratios of upstream (reservoir) and downstream (atmosphere or tailwater) conditions. If the figure is interpreted as representing a cross section of a horizontal nozzle through which gas is flowing from left to right, the different parts of the figure represent the flow field from different high pressures ($P_1, P_2, \ldots$) in the left reservoir. The gas flows into an infinitely large reservoir (not shown) at lower pressure on the right. Alternatively, if Fig. 2 is interpreted as representing a map view of a horizontal channel in which shallow water is flowing from left to right, the different parts of the figure represent the

flow field from reservoirs of different depth. The driving energy for the flow is the elevated depth of water in the left reservoir compared with the right. The water has a potential energy, H_r, called the *head* and generally expressed as a depth, indicated as $H_1, H_2, \ldots$ in the parts of Fig. 2.

With this introduction, let us reexamine the sense in which each of the geologic problems mentioned above is a nozzle problem[5]. The nozzle of the Colorado River is the river channel, a converging-diverging nozzle formed by debris flows that constrict the main channel, and the fluid is shallow water. The "geologic twist" that complicates simple application of flume concepts is that the walls and bed of the channel are erodible, and the channel can therefore change shape in response to changing conditions in the flow. The nozzle of Old Faithful geyser is a fissure of irregular (and largely unknown) geometry extending more than 20 m into the ground. The geologic twist in this problem is that the fluid is much more complex than a perfect gas: hot, liquid water stands in the conduit between eruptions, and then boils and changes through a complex unloading process into a droplet-laden steamy aerosol during an eruption. The nozzle of the Mount St. Helens lateral blast was a huge vent created when a landslide caused by an earthquake opened a vertical scarp nearly 0.25 km^2 in area and exposed a hot, hydrothermal, magmatic system. The erupting fluid was a hot vapor heavily laden with ash, rocks, ice fragments, and tree debris. As these three examples show, the scale of the geologic nozzles is large, the nozzle shapes are irregular, and the thermodynamic properties of the flowing fluids are complex.

II. Sound velocities and critical velocities: their influence on the flow field

The most important result from the above analogy is the recognition that characteristic velocities control flow behavior in shallow water and gas flow. For small disturbances, the equations of momentum (Eqs. (7) and (9)) can be linearized and written as

$$\frac{\partial^2 P}{\partial t^2} - a_o^2 \frac{\partial^2 P}{\partial x^2} = 0 \qquad \text{(perfect gas)} \tag{10}$$

and

$$\frac{\partial^2 h}{\partial t^2} - g\, h_o \frac{\partial^2 h}{\partial x^2} = 0 \qquad \text{(shallow water)}\,. \tag{11}$$

These are the well-known *wave equations*, from which it can immediately be seen that small disturbances propagate with characteristic velocities proportional to the square root of the coefficient of the second term. In compressible gas flow, the characteristic velocity is the *sound velocity*, a_o, the velocity at which small perturbations in density or pressure propagate through the fluid:

$$a^2 = \left(\frac{\partial P}{\partial \rho} \right)_S , \tag{12}$$

where the derivative is taken at constant entropy, S. In shallow-water flow, the characteristic speed is the *critical velocity* -- the velocity of a gravity wave of long wavelength and infinitesimal strength:

$$c^2 = g\, h \ . \tag{13}$$

In both cases, the nature of the flow field depends on the magnitude of the fluid velocity compared with the characteristic velocity. The *Mach number*, M, of a compressible gas flow is the ratio of the mean flow velocity to the sound speed:

$$M = u/a \ . \tag{14}$$

The *Froude number* of shallow water flow, Fr, is the ratio of the mean flow velocity to the critical velocity:

$$Fr = u/c \ . \tag{15}$$

The local flow variables are determined by these dimensionless ratios, which, in turn, depend on reservoir conditions and geometry. For gas flow, the important parameters are the ratio of the pressures in the driving and receiving reservoirs, the area ratio along the axis, and the gas equations of state (particularly R and γ for a perfect gas). For shallow-water flow, the important parameters are the ratio of upstream to downstream energy and the area ratio of the channel. Depending on the values of these parameters, the flow field can have dramatically different properties, as illustrated in Fig. 2.

Consider, first, that Fig. 2 represents the flow of gas through a nozzle. When the pressure P_1 in the reservoir is "low" [6], the fluid accelerates from the reservoir into the constriction and decelerates in the diverging section (Fig. 2a). This is the classic *venturi tube*, and the flow is everywhere *subsonic*.

If the pressure ratio is higher (Fig. 2b), the fluid accelerates from the reservoir into the converging section and can reach *sonic* or *choked* conditions ($M = 1$) in the throat; it can be rigorously shown that sonic conditions can only occur in the throat. At one particular pressure ratio the flow can decelerate back to subsonic conditions in the diverging section, but for higher values it will accelerate to *supersonic* conditions in the diverging section. Strong nonlinear waves -- *shock* and *rarefaction waves* -- can be present and are, in fact, usually required to decelerate the flow back to ambient conditions in the exit reservoir. At pressure ratios for which supersonic flow conditions are obtained, a *normal shock* stands in the diverging section and the deceleration to ambient conditions occurs within the nozzle between the shock and the exit plane (Fig. 2b). At still higher pressure ratios (Figs. 2c and 2d) the shock is "blown out" of the

nozzle, and a complicated flow field consisting of oblique and normal shocks and mixed regions of subsonic and supersonic flow exists within the exiting jet. Because the decelerating waves are nonlinear, the jet "overshoots" ambient conditions and multiple shock and rarefaction waves are required to achieve the pressure balance[7].

Consider alternatively that Fig. 2 represents shallow-water flow. When the head difference between the reservoirs on the left and right is "small" [8], the flow is *subcritical* everywhere -- the fluid accelerates in the converging section and through the constriction, and decelerates in the diverging section (Fig. 2a). The flow field is analogous to that in a venturi tube. The word *streaming* is often used for subcritical flow.

If the head ratio is greater, as indicated in Fig. 2b, the flow accelerates from the reservoir through the converging section and can reach *critical* conditions ($Fr = 1$) in the constriction. At the critical value of head ratio the flow can decelerate to subcritical conditions in the diverging section, but for other higher values it will accelerate to *supercritical* conditions in the diverging section. The word *shooting* is often used for supercritical flow. Strong nonlinear waves, in this case called *oblique* (or *slanting*) and *normal hydraulic jumps*, are generally required to decelerate the flow back to ambient conditions in the downstream reservoir. Depending on the head ratio and the severity of the constriction, waves can stand in (Fig. 2b) or downstream of (Figs. 2c and 2d) the diverging section[9].

The flow fields shown in Fig. 2 are a subset of possible flow conditions, for they do not show possible wave structures that arise if fluid enters the constricted part of the nozzle in a supersonic or supercritical state. Such conditions can, in fact, be obtained geologically. For example, if a change in river-bed elevation causes water to accelerate to supercritical conditions before a lateral constriction is encountered, the flow can be supercritical as it enters the convergence, rather than subcritical as illustrated in Fig. 2. For simplicity, this complexity is ignored in this paper.

Supersonic or supercritical conditions are amazingly easy to obtain in geologic settings. If the ratio of reservoir pressure to atmospheric pressure in a gas nozzle is more than about 2, sonic and supersonic flow will occur in the nozzle; for comparison, the ratio of pressure in a volcanic reservoir to atmospheric pressure is often around 100 : 1. If shallow water flows from one reservoir to another that has less than 2/3 of the head of the source reservoir, critical conditions can be obtained in the throat; for comparison, backwater depths on the Colorado River may exceed downstream tailwater depths by a factor of 2. Thus, the existence of supersonic or supercritical flow fields in geologic settings is conceptually reasonable.

Our intuition, however, generally fails to prepare us for the possibility of such flows in the natural world. We commonly think of supersonic flow in terms of modern aeronautics: objects obtain high Mach numbers by moving very fast through air, which

has a high sound speed. Geologic fluids rarely move at the speeds characteristic of modern aircraft (except in some volcanic eruptions), but the entire spectrum of flow behavior from subsonic to supersonic (and subcritical to supercritical) can occur in geologic flows because the fluids can have very low characteristic velocities. Fluids with low sound velocities can develop internally supersonic flow fields while still moving subsonically with respect to the surrounding atmosphere. That is, there can be standing shock or rarefaction waves internal to the flow, but no standing waves in the external medium.

Fluids in geothermal and volcanic settings typically have low sound speeds: water that contains gas bubbles (e.g., air or CO_2) or steam bubbles (boiling water) has a very low sound speed, because the gas bubbles dramatically increase the compressibility of the mixture, κ_S. An alternative form of the definition of sound speed, $a = (1/\kappa_S)^{1/2}$, shows this dependence clearly. The sound speed in an air-water mixture can be as low as 20 m/s. The sound speed is further decreased in a mixture in which the bubbles are of the same composition as the liquid (e.g., steam bubbles in boiling water), because exchanges of mass and latent heat accompany passage of a sound wave; these exchange processes also decrease the sound velocity. Sound speeds as low as 1 m/s are possible for boiling water[10].

The dependence of sound speed on phase, and on pressure and temperature, can be shown on an entropy-density (S-ρ) phase diagram[11] (Fig. 3). This representation is suggested by the definition of sound speed given in Eq. (12) above: on a graph of density versus entropy, sound speed is proportional to the vertical gradient of isobars. Such a graph can be read as an ordinary topographic map on which "flatlands" represent low sound speeds and "cliffs" represent high sound speeds (shown schematically in the inset in Fig. 3). The S-ρ representation shows the wide range of sound speeds characteristic of simple one-component substances. If such fluids flow from high to low pressure (e.g., in eruptions or in geo-thermal wells), the phase of the fluid can change from liquid to liquid + vapor, or from vapor to vapor + liquid. A hypothetical decompression path appropriate to Old Faithful (and discussed later in Section IV) is shown as the vertical line (a) in Fig. 3. Note that along this decompression path the sound speed can change by several orders of magnitude. If the fluid is in a two-phase state, flow velocities of only a few tens of meters per second can give a wide range of Mach numbers, including sonic ($M = 1$) and supersonic ($M > 1$) flow.

Mass loading of vapor with solids or liquid droplets also produces fluids with low sound speeds. No data or theories exist for the fluids encountered in volcanic problems, where, for example, the mass ratio of solids to vapor can exceed 100, and particle sizes within a single flow can range from microns to meters. At present, we can only apply simple pseudogas theory to this problem to obtain characteristic sound speeds (Fig. 4). Sound speeds of 50 to 100 m/s are plausible. Flow velocities in gassy volcanic eruptions are commonly on the order of 100 m/s and can exceed 500 m/s. Therefore, a wide range of Mach numbers, including $M > 1$, can be obtained.

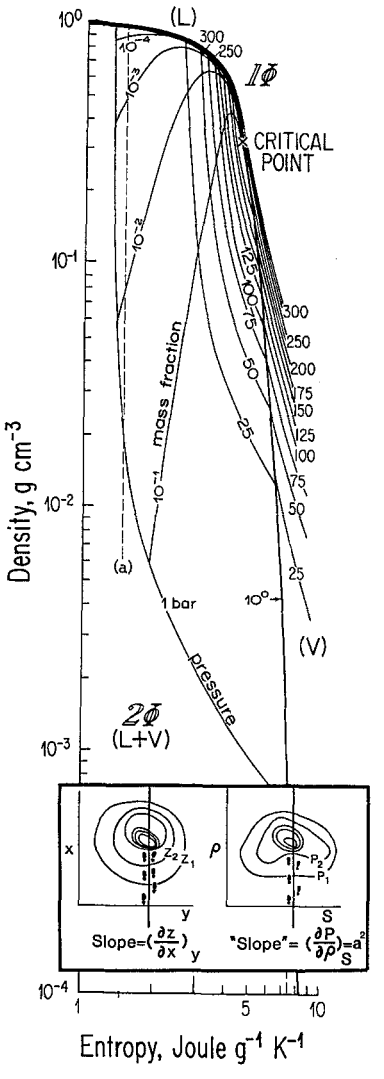

FIG. 3. The entropy-density ($S - \rho$) phase diagram[11] for H_2O. Entropy is relative to the triple point of H_2O. The label 1ϕ marks the single-phase field and the label 2ϕ marks the two-phase field (liquid + vapor). Contours of constant pressure (isobars) are shown in 25-bar increments. In the two-phase field, contours of constant mass fraction of vapor (isopleths) are shown. A similar graph for CO_2 can be found in Ref. 11. The vertical dashed line (a) represents an isentropic path that might be taken by a fluid decompressing from the bottom of Old Faithful. The horizontal inset is a comparison of a standard topographic map of a conical hill (left) with the entropy-density graph used to illustrate sound speed. The spacing of the contours is inversely proportional to the steepness of the topography in the case of a map (left), and to the sound speed in the case of an $S - \rho$ diagram (right). In the latter case, the "footsteps" indicate that the appropriate derivative for considering sound speed is in the vertical direction.

Finally, note that the critical velocity in shallow-water flow plays the same role as the sound speed in determining transitions between linear and nonlinear flow regimes. Critical velocities in rivers can be of the order of the flow velocities, even in major rivers where large depths increase the critical velocity (Eq. 13). In the Colorado River in the Grand Canyon, for example, water depths of the order of 10 m are common; the corresponding critical velocity is 10 m/s. In most calm stretches of the river, flow velocities are on the order of 1 m/s, and Froude numbers are less than 0.1. In major rapids, however, where the water becomes shallow and fast, the flow velocity can exceed the critical velocity ($Fr > 1$). Supercritical flow is not common in rivers[12], but when it does occur, the geologic consequences can be great; one such case is discussed in the following section.

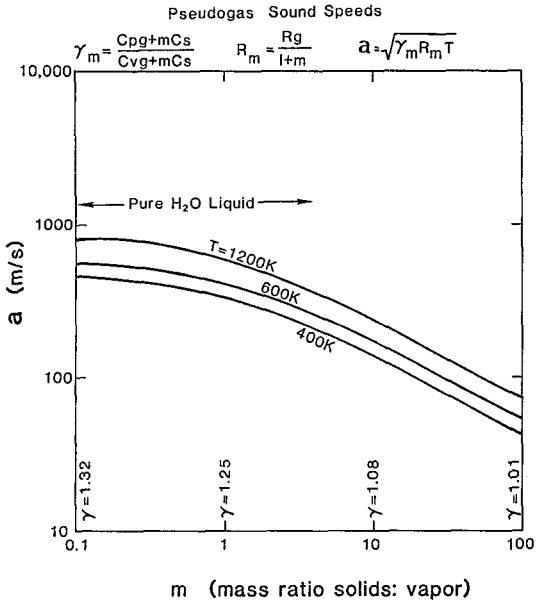

FIG. 4. Sound speed, a, of pseudogas versus mass ratio, m, of solids to vapor (steam). Curves for three different temperatures spanning the range of geothermal and volcanic interest are shown. The sound speed of pure liquid water is indicated. The isentropic exponent, γ, varies with m as indicated at the bottom of the graph. Because the mass loading is high (of order 10, say) in many volcanic eruptions, γ is near unity.

Many simplifications have been made in the discussion above, and these, as well as others, will be used in the analyses below: e.g., thermodynamic equilibrium; isentropic, quasi-one-dimensional flow; steady flow; and perfect gas or pseudogas behavior. One additional major simplification in the following analyses is that the flow fields are assumed to be *either* compressible and gravity-free ($M > 1$, $Fr > 1$), or gravity-dominated and incompressible ($Fr < 1$, $M < 1$). The assumption of incompressible shallow-water flow is good for the Colorado River. However, compressibility and gravity are probably both important for the flow fields of Old Faithful and the Mount St. Helens lateral blast (i.e., $M > 1$, $Fr < 1$)[13]. This complex problem is only beginning to be addressed as the capabilities of modern supercomputers are being turned toward the problem.

III. Crystal Rapids: subcritical and supercritical flow in an erodible channel

A. Geologic setting and the events of 1983

The Colorado River is the largest of the great rivers in western America. In the 400-km stretch through the Grand Canyon, numerous debris fans have been deposited

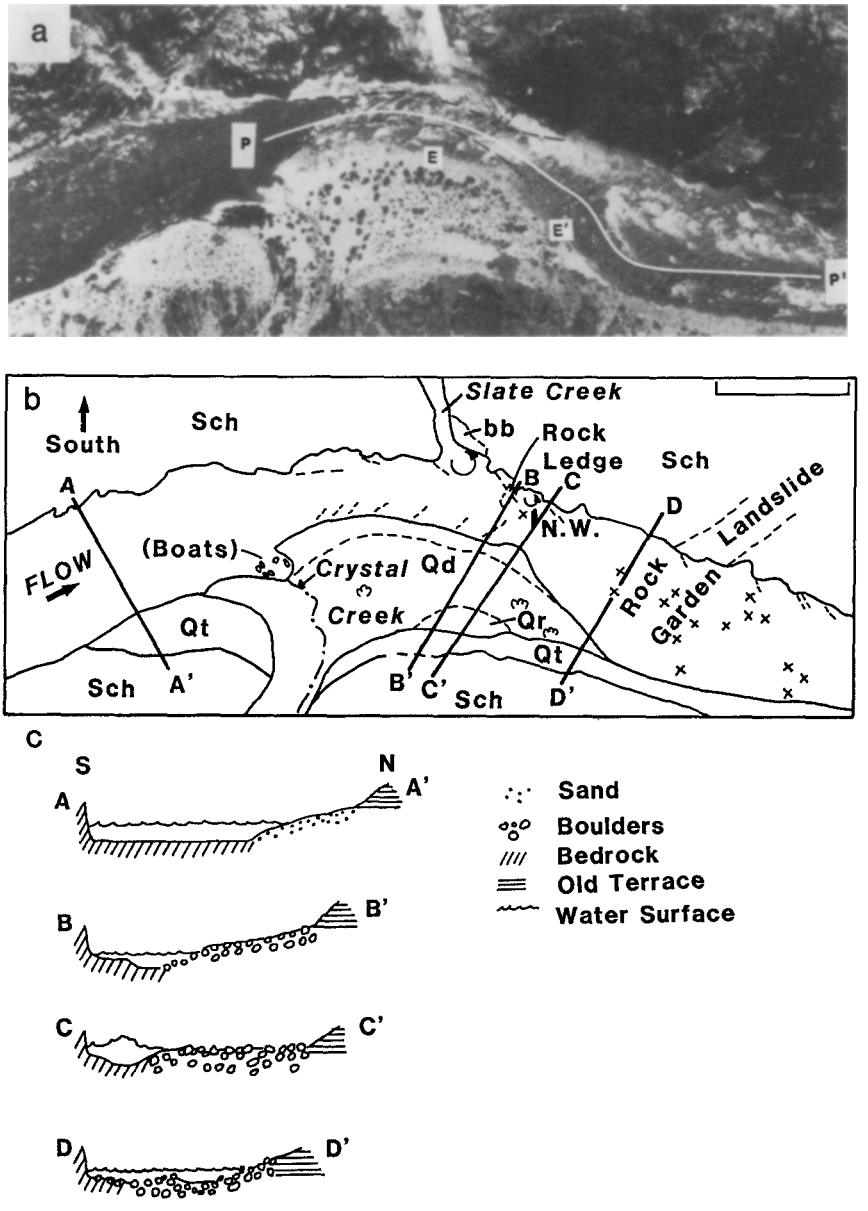

FIG. 5. (a) and (b) Crystal Rapids at two dramatically different discharges. (c) and (d) Keys to features in (a) and (b). (a) June 16, 1973 (U.S. Geological Survey Water Resources Division air photo). The discharge in (a) was about 283 m^3/s (10,000 cfs); the discharge in (b) was 2,600 m^3/s (92,000 cfs). The rise of the river shoreline from the lower (southern) end of the debris fan in (a) to the base of the old alluvial terrace in (b) represents a stage change of about 5.5 m. Note the constriction of the river channel as it passes downstream from left to right through the debris fan, and the expansion downstream of the debris fan. In the downstream region (beginning approximately at the inflection point on the right half of PP′ and extending past P′ in (a)), the channel

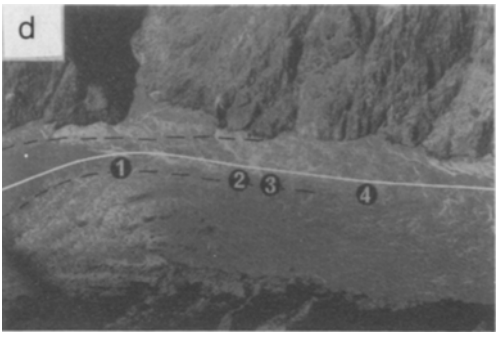

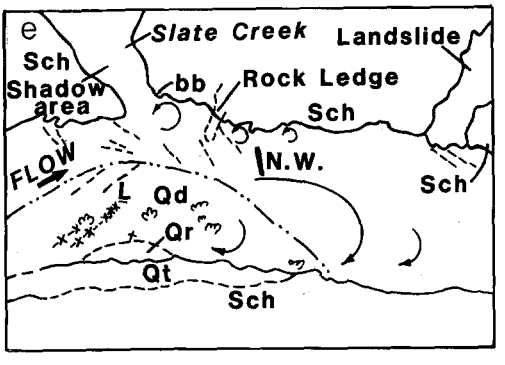

C EXPLANATION

Qd - 1966 debris fan

Qr - Older debris fan

Qt - Older terrace

Sch - Schist

X - Rock or rock-caused wave (I)

--- Oblique wave (II)

— Normal wave (III)

Eddy

A —— A',etc., Cross sections

—L Stranded log in (b)

bb - Boulder-bar

Tamarisks

FIG. 5. (continued)

bottom is littered with boulders (the "rock garden" whose origin is discussed in the text). Rocks in the rock garden are visible at 283 m^3/s (10,000 cfs) as shown in (a), cause substantial waves at 30,000 cfs, and are submerged at 2600 m^3/s (92,000 cfs) as shown in (b). PP′ was the preferred navigation route prior to 1983. The normal hydraulic jump of interest in this paper (indicated by NW in (c) and (d)) is not easily visible in the two photographs, both because of the large area covered by the photos and because turbulence and many small waves cause variations in the reflectivity of the features on the water. The wave can be seen in detail in Fig. 7. (c) Schematic cross-sections. The relative widths are correct; the vertical scale is arbitrarily exaggerated. The important points to note from the cross sections are the small cross-sectional areas at BB′ caused by high velocities in the constricted part of the rapid, and the greater depth in CC′ caused by the hydraulic jump (shown schematically as an exaggerated wave on the water surface).

by flash floods in tributary canyons (Fig. 5). Flash floods in the tributaries can carry boulders many meters in diameter into the path of the Colorado River, because the gradient of the tributaries is quite steep. When emplaced, the large debris fans temporarily obstruct the path of the river, damming it until the debris deposit is breached and a new channel carved. The major rapids on the Colorado River are located where the river passes through these debris fans.

The channel of the Colorado River resembles a converging-diverging nozzle in the vicinity of these debris fans (note the constriction of the channel in Fig. 5). Typically, the channel narrows from a characteristic upstream width of about 100 m to a narrowest point in the "throat" of the rapid, and then diverges back to a downstream width about equal to the upstream width (e.g., Fig. 5). The ratio of the width of the river at the throat to the width at an average upstream section is the *constriction* of the river; I will also refer to it as a "shape parameter." Constrictions at the debris fans in the Grand Canyon are remarkably uniform at a value of about 0.5 (Fig. 6). There is no *a priori* reason to believe that the debris fans themselves were emplaced in such a way that, by coincidence, half of the main channel was blocked. What, then, is the significance of this characteristic nozzle shape? It must be telling us something about the ability of the Colorado River to erode its own channel, i.e., to contour its own nozzle.

Because the debris fans are generally very old (of the order of 10^3 to 10^5 years) and because the flash floods that create and renew them are rare, we have little hope of observing the processes that create the balances between tributary floods and main channel erosion. However, a unique series of events spanning the two decades from 1966 to 1986 has given us a glimpse of these processes. In January, 1963, Glen Canyon Dam at Page, Arizona (Fig. 7) was closed, and the discharge into the Colorado River through the Grand Canyon became controlled by demands for electrical power and water storage at the dam, rather than by natural flooding. About four years after the dam was closed, a flash flood down Crystal Creek emplaced a large debris fan across the river about 175 km below the dam (Fig. 5). There were no witnesses to this event;

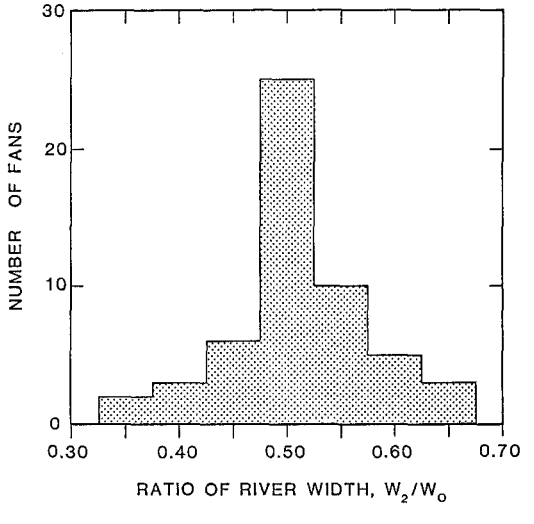

FIG. 6. Histogram of constriction values (shape parameter) for the Colorado River as it passes 54 of the largest debris fans in the 400-km stretch below Lee's Ferry, Utah. These values are based on the widths of the *surface* water in the channel in 1973 air photos (such as shown in Fig. 5).

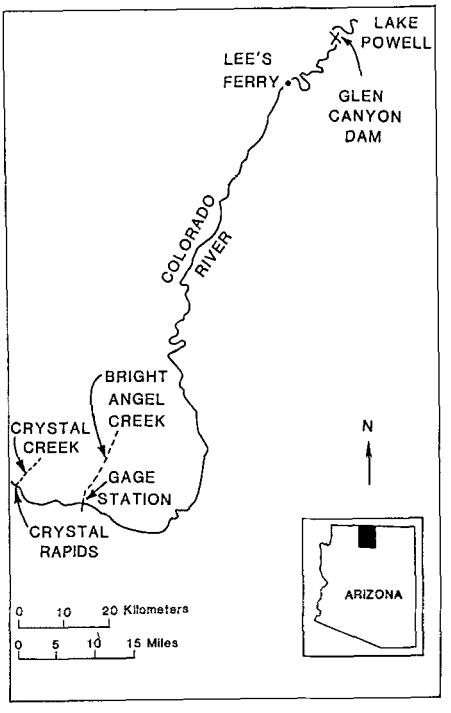

FIG. 7. Index map for locations near Crystal Rapids.

by the time observations were made, the Colorado River had carved a channel through the distal (south) end of the debris fan. When first measured (on the 1973 air photograph shown in Fig. 5), the constriction of the river channel through the fan[14] was roughly 0.33, substantially more severe than the constrictions of the more mature fans along the Colorado River. From 1966 to 1983, the discharges through the dam were held below 850 m^3/s (30,000 cubic feet per second (cfs))[15], and the constriction remained at about 0.33.

The water surface of the Colorado River became very rough and turbulent as it passed through the Crystal debris fan -- this stretch of water, nearly 1 km long, is known as Crystal Rapids. The boulders, waves, and eddies in Crystal Rapids made it one of the two most difficult stretches of the river for raft navigation, even at the normal levels of controlled discharges between 1966 and 1983 (140 m^3/s (5,000 cfs) to 850 m^3/s (30,000 cfs)). The rapid is a major hazard for recreational rafting, an activity in the Grand Canyon involving about 10,000 people each year. Between 1966 and 1983, the major navigational obstacle occurred where water poured over a large rock into a deep hole and emerged through a sharp-crested wave in the narrowest part of the rapid. This feature was known as the "Crystal Hole" (the location of the Crystal Hole is shown in Fig. 5, but the feature itself is too small to show at the scale of this photograph).

At low discharges, a rock about 2 m high was seen as the cause of this hydraulic feature, and the significance of this rock relative to the significance of the severe

constriction was, in hindsight, overestimated. Many waves in the rapids of the Colorado River are caused by large rocks. River guides who ran the river before Glen Canyon Dam was closed, when large natural floods reached 2,300 to 3,600 m^3/s (80,000 to 125,000 cfs) annually, reported that, in most rapids, the waves became very weak or disappeared ("washed out") at high discharges because the obstacles causing them became submerged ("drowned"). There was, however, no record of the behavior of waves in Crystal Rapids at discharges exceeding 850 m^3/s (30,000 cfs), because the rapid -- in its modern severe form -- did not exist before construction of Glen Canyon Dam.

In 1983, rapid snow melt in the headwaters of the Colorado River forced the Bureau of Reclamation to increase discharges through Glen Canyon Dam to 2,600 m^3/s (92,000 cfs) to prevent Lake Powell from flowing over the dam. As discharges increased above 850 m^3/s (30,000 cfs) -- a level that had not been exceeded for two decades -- the waves in most rapids disappeared, as expected. The rapids "drowned out" and the river ran smooth and fast through most of the Grand Canyon.

This was not the case at Crystal Rapids: as the discharge reached 1,700 to 2,000 m^3/s (60,000 to 70,000 cfs), a wave reported by experienced boatmen to have been as high as 9 m, and photographically documented to have exceeded 5 m, stood across most of the river channel (Fig. 8). At greater discharges the height diminished -- at 2,600 m^3/s (92,000 cfs) the wave surged only between 3 and 5 m. Because typical river rafts are 5 to 11 m in length and 2 to 4 m in width, the wave was a severe obstacle to boating. One rafter was drowned, and dozens of others were seriously injured. The National Park Service closed the rapid to commercial boating until the discharges were decreased. The existence of this large wave at high discharges, and its evolution with changing discharge, provided clues about the relation between the Colorado River and its debris fans.

B. Results of analysis of shallow-water flow

Certain aspects of the flow in the rapids of the Colorado River can be analyzed in terms of conservation of mass and momentum for flow in a converging-diverging channel[16]. As discussed in the context of Fig. 2, the shape of the channel, and the upstream and downstream reservoir heads, must be specified. The river channel, which is actually very irregular in shape (Fig. 5c), is simplified to be rectangular in cross-section for the analysis. This simplification causes the shape parameter (the average constriction) to be 0.25, instead of the value 0.33 measured from the surface width of the water.

Six different flow zones can be identified, as shown in Fig. 9a: (0) an upstream state of unconstricted, uniform flow; (1) the convergent section of the channel upstream from the constriction; (2) the constriction; (3) the beginning of the divergence; (4) the end of the divergence; and (5) a downstream state of uniform flow not influenced by the constriction. Regions (3) and (4) may be separated by a hydraulic jump.

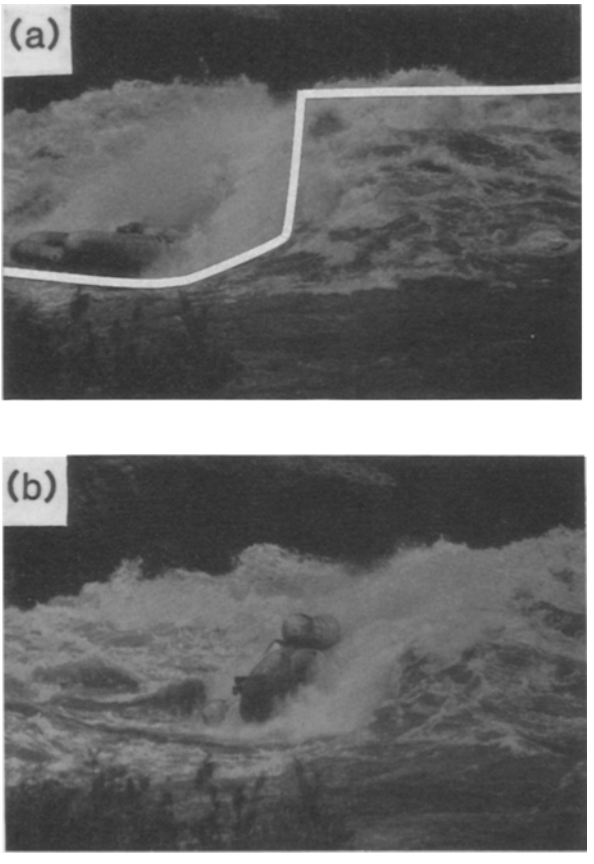

FIG. 8. River raft (a) entering and (b) trapped in the large wave at Crystal Rapids on June 25, 1983, when the discharge was approximately 1,700 m^3/s (60,000 cfs). Photographs copyrighted by Richard Kocim; reprinted with permission. The pontoons on the raft are each 1 m diameter; the midsection is about 3 m diameter. More than 30 passengers are on board; one head is visible on the lower left side of the raft in (b). To aid the reader in distinguishing the water surface in the foreground and near the boat from turbulent water in the background, a white line has been drawn along the approximate surface of the water upstream from and through the hydraulic jump in (a). From the scale of the raft, the trough-to-crest height of the wave can be estimated to exceed 5-6 m.

Water flows through the rapid because the upstream reservoir is higher than the downstream reservoir. In a notation slightly changed from that used in the general equations of Section I, to be consistent with Fig. 9b, application of the Bernoulli equation to any two cross sections 1 and 2 gives the total energy balance as

$$z_1 + D_1 + \frac{u_1^2}{2g} = z_2 + D_2 + \frac{u_2^2}{2g} + E \ , \tag{16}$$

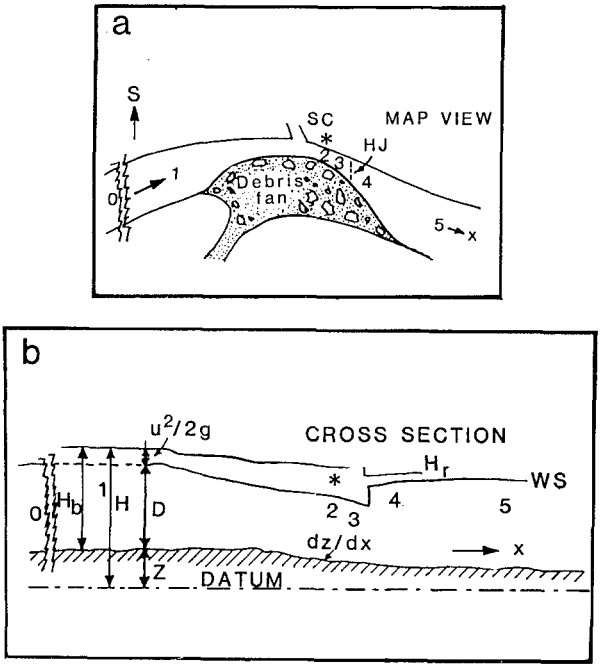

FIG. 9. (a) Schematic map view of the river and the debris-fan configuration at Crystal Rapids. The debris fan at the bottom of the map emanates from Crystal Creek. SC indicates the position of the other tributary, Slate Creek. The regions 0, 1, 2, 3, 4, 5 are defined in the text. HJ indicates a possible hydraulic jump. (b) Schematic longitudinal profile, showing the notation used in the energy relation given in the text and in Fig. 10.

where E is the energy dissipated between sections 1 and 2. (The change in convention from the variable h used in Section I for water depth to the variable D is required to account for a sloping channel bottom by referencing both the channel bottom and the water surface to a datum plane, as in Fig. 9b). For simplicity, and because of a paucity of data, the energy change due to the change in bed elevation $(z_1 - z_2)$ is assumed to be compensated by energy dissipation in the flow, E. This assumption allows the flow to be considered at constant *specific energy* $(D + u^2/2g)$, except across hydraulic jumps. For the analysis, the discharge variation of the specific energy of the unconstricted flow upstream of Crystal Rapids was estimated from measurements at a U.S. Geological Survey gage station 16 km upstream at Bright Angel Creek (Fig. 10a, heavy line, H_r). The flow below Crystal Rapids was assumed to return to this same specific head.

The flow entering the rapid can have the ambient specific head, H_r, if and only if all of the discharge can be accommodated through the constriction. If the constriction is

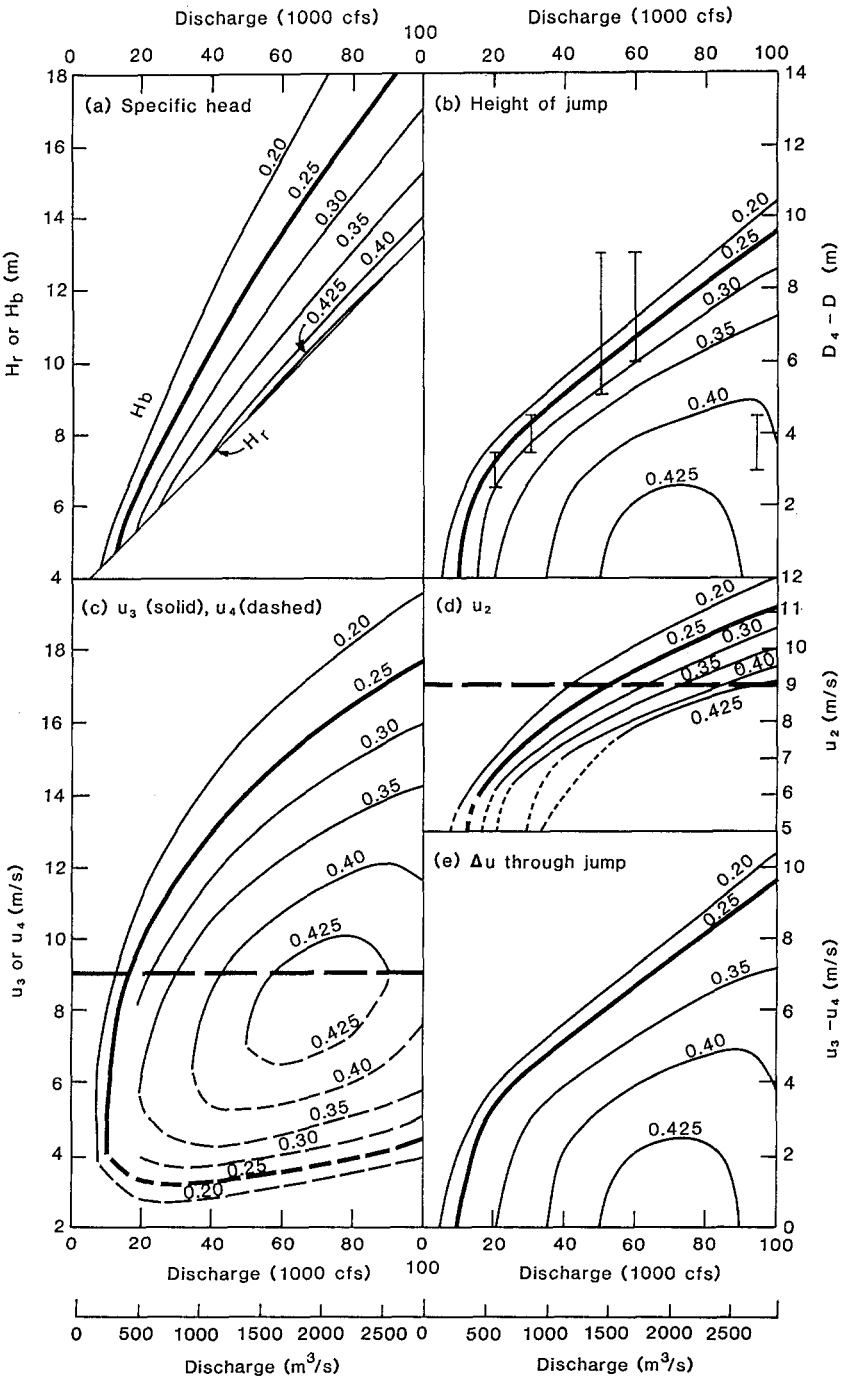

FIG. 10. Summary of the shallow-water flow calculations for Crystal Rapids given in Kieffer[16]. Subscripts on the various parts of this figure refer to regions defined in the text and shown schematically in Fig. 9; e.g., u_2 is the flow velocity in flow zone 2. In

all sections of this figure, the curve appropriate to the initial constriction at Crystal Rapids, 0.25, is shown by a heavy line. (a) Specific head, H_r, of the unconstricted river versus discharge. The curves labeled H_b are the backwater heads that develop upstream of Crystal for conditions of critical (choked) flow. The backwater head depends on the constriction and is given for values ranging from 0.20 to 0.425, as labeled on the curves in this and all other parts of the figure. (b) The curves show the calculated height of the hydraulic jump that separates regions 3 and 4 when supercritical flow occurs; the constrictions are indicated on each curve. The bars are values observed during the 1983 flood. (c) The solid curves (top) are calculated values of the flow velocity in the diverging section of the channel (region 3) immediately upstream of the hydraulic jump. The dashed curves (bottom) are calculated values of the flow velocity in the diverging section of the channel (region 4) immediately downstream from the hydraulic jump. The horizontal dashed line at 9 m/s indicates the velocity at which larger boulders at Crystal Rapids can probably be moved by the current. (d) Calculated Calculated values of velocity in region 2, the constriction. The flow is subcritical where the curves are dashed. (e) Calculated decelerations through the hydraulic jump that separates regions 3 and 4.

---

too severe, the ambient head of the flow, H_r, may not be sufficient to allow the discharge to be accommodated through the constriction. In such cases, critical conditions occur in the constriction, and a *backwater* is required upstream. The deepening of the backwater increases the specific head of the flow over that in the unconstricted part of the channel and permits a greater discharge per unit area through the constriction. The calculated backwater head, H_b, compared to the ambient river head, H_r, is shown as a function of discharge, Q, and constriction value in Fig. 10a. Note from this figure that, for a constriction of 0.25, a backwater head is required for all discharges over about 300 m^3/s (~ 10,000 cfs)[17]. This means that supercritical flow will occur in the rapid at discharges above this value.

Solutions of the shallow-water flow equations (Figs. 10 and 11) show that Crystal Rapids went through the entire spectrum of nozzle behavior shown in the sketches of Fig. 2 as discharges increased during the 1983 flood[18]. At discharges below about 300 m^3/s (~ 10,000 cfs) the flow was essentially subcritical[19] (curve A in Fig. 11). At higher discharges the flow became critical, and then highly supercritical (curves B-E in Fig. 11).

A hydraulic jump is required in the diverging section of the rapid to decelerate the supercritical flow and to drop its energy from the backwater head, H_b, back to the ambient downstream head, H_r. Thus, the model suggests that the large wave that stood in the diverging section of Crystal Rapids at high discharges can be interpreted as a normal hydraulic jump arising from the severe constriction of the channel (Fig. 2). In hindsight, this wave can be recognized as having been present all through the 1966-1983

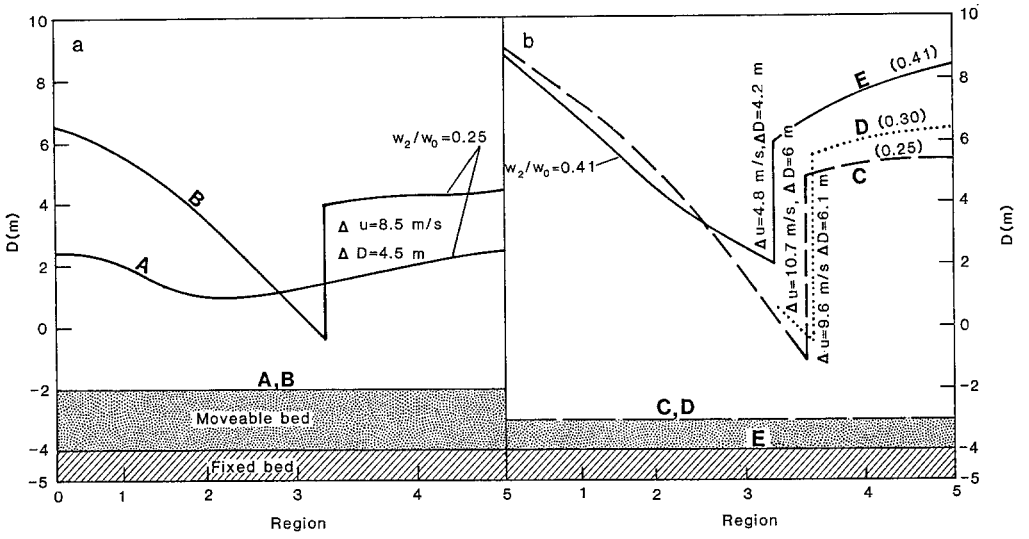

FIG. 11. Schematic longitudinal water profiles at Crystal Rapids for the 1983 discharges up to 2,550 m^3/s (90,000 cfs), showing the effect of channel widening and bed erosion on the height of the hydraulic jump. The parts of the rapid defined in the text and in Fig. 9 (regions 0-5) are shown schematically by the labels below the graph. Each curve represents a different discharge and may be related to a different bottom level, depending on the erosion presumed to have taken place. For example, curves A and B are for discharges of 283 m^3/s (10,000 cfs) and 850 m^3/s (30,000 cfs), respectively, and show the water surface relative to the top of the movable bed labeled A,B. Curves C, D, and E are for discharges of 1,400 m^3/s (50,000 cfs), 1,700 m^3/s (60,000 cfs), and 2,550 m^3/s (90,000 cfs), respectively. Each curve shows the water surface relative to the bed labeled with the same letter; the base level of the bed changes because of erosion, as discussed in the text. Each curve is labeled with the constriction assumed to apply during the 1983 discharges. For the conditions under which supercritical flow occurs (curves B-E), the height of the hydraulic jump and the velocity change across it are given beside the vertical line representing the jump.

phase of Crystal Rapids. However, because the large rock in this vicinity acted like a small-scale natural weir, the energy change of the flow around the rock contributed substantially to the energy of the wave at low discharges, so that the role of the constriction was not recognized. Only when the wave strengthened with increasing discharge, rather than washing out, was the role of the constriction recognized.

As the discharge through Glen Canyon Dam rose from 850 m^3/s (30,000 cfs) to about 1,700 m^3/s (60,000 cfs) in June, 1983, the height of the wave increased, as would be expected for a hydraulic jump in a channel of fixed geometry (Fig. 10b; compare the left four data bars with the heavy curve). At higher discharges, however, the height of the wave *decreased*, rather than increasing as predicted by the calculations (Fig. 10b; compare the right data bar with the heavy curve).

This puzzling observation can be explained if the magnitudes of the flow velocities in the constriction and upstream of the hydraulic jump are examined (Figs. 10c and 10d; see also the profiles in Fig. 11). In supercritical flow, water accelerates in the converging section of the nozzle, reaching critical velocity, u_2, in the throat. The water continues to accelerate out the diverging side of the constriction, reaching a maximum velocity, u_3, immediately upstream from the hydraulic jump. A sudden deceleration to velocity u_4 occurs across the hydraulic jump as the flow deepens. For example, at a discharge of 1,400 m^3/s (50,000 cfs), with a constriction of 0.25, the calculated velocity in the constriction, u_2, is 9 m/s and the velocity increases to $u_3 = 14$ m/s just upstream from the hydraulic jump (Figs. 10c and 10d). The velocity decreases to $u_4 \sim 3$ m/s just downstream from the jump.

Consideration of the Hjülstrom criterion for particle movement and of unit stream power shows that water moving at 9 m/s can move boulders that are 1-2 m in diameter, the characteristic size of the large boulders of the Crystal debris fan. Therefore, when velocities reached this magnitude (at discharges in the range of 1,400 to 2,000 m^3/s (50,000 to 70,000 cfs), as shown in Fig. 10), large scale erosion began; that is, the river was able to begin contouring its own nozzle. Material was eroded from the sides of the channel and from the river bottom. Vertical erosion scoured the channel in an upstream direction (headward erosion); lateral erosion increased the width of the throat. An observer standing on the shore could not see this erosion taking place, but could hear loud, bass booms as boulders moved in the current.

Channel widening at the throat can account for the observed decrease in height of the hydraulic jump. Comparison of the observed wave height with that predicted for a normal hydraulic jump as the discharge changed from 1,700 m^3/s (60,000 cfs) to 2,600 m^3/s (92,000 cfs) suggests that the channel widened from a shape parameter of 0.25 to about 0.40-0.42, a widening of 12-13 m (Fig. 10b). The location of this erosion is shown in the photograph of Fig. 12.

In summary, a fascinating, and often tense, feedback process involving meteorology, river hydraulics, and engineers began in June 1983 and continued into early July as the discharge increased; this process can be followed on the curves of Fig. 10. As snow melted in the Rocky Mountains, engineers raised the discharge through the dam higher than the 850 m^3/s (30,000 cfs) released during the previous two decades. At the tightly constricted spot in Crystal Rapids, a large hydraulic jump formed because the flow became highly supercritical. As the discharges approached 1,700 m^3/s (60,000 cfs), the river began eroding its channel through the Crystal Creek debris fan. In response to the widening, the flow velocities decreased. If the discharge had been held constant, the channel and hydraulic features of the flow would have stabilized when the channel became wide enough to reduce flow velocities in all sections below about 9 m/s. However, more snow melted in the headwaters of the Colorado River, and engineers were forced to increase discharges through the dam toward 2,600 m^3/s (92,000 cfs). In

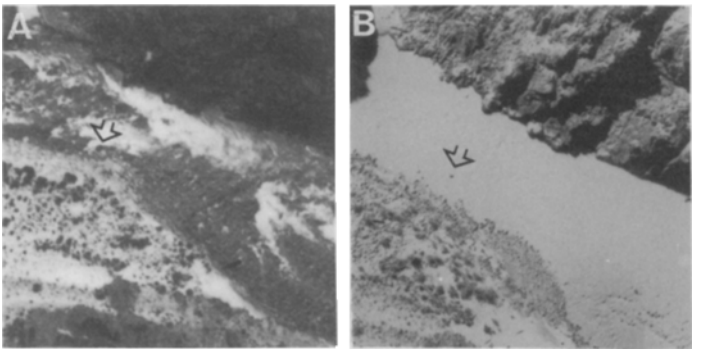

FIG. 12. (a) and (b) Comparison of the shore line at Crystal Rapids (a) before and (b) after the 1983 high discharges. The arrow indicates a large rock visible for reference in both photos. The discharge in (a) is about 283 m^3/s (10,000 cfs); in (b) it is about 170 m^3/s (6,000 cfs). Note the widening of the channel immediately downstream (right) of the indicated rock. Even though the discharge is lower in (b) than in (a), boats can be seen in an "alcove" in (b) which they could not have reached under the conditions present in (a). The shore where this erosion has taken place is the channel boundary along regions 2 and 3 where the flow velocities were the highest during 1983. In the field, a cut bank nearly 2 m in height can be traced from the left side of (b) to the boats.

response to the increased discharge, flow velocities again increased, and erosion of the channel continued; by the time of peak discharge, enough lateral erosion of the channel had occurred that the height of the hydraulic jump had decreased. It is not clear at this time whether the high flows were sustained long enough for the channel to take on a shape in equilibrium with the high discharge.

C. Implications for geomorphic evolution in the Grand Canyon

Even after the channel was widened by the high discharges of 1983, the constriction of 0.40-0.42 at Crystal Rapids is still significantly below the value of 0.5 characteristic of the mature debris fans along the Colorado River (Fig. 6), and the rapid is significantly different in hydraulic character from rapids at locales where the constriction is 0.5. This observation suggests that most debris fans in the Grand Canyon have been subjected to floods larger than the 1983 flood. With proper recognition of the simplicity of the model and the paucity of data, extrapolation of calculations at Crystal Rapids can be used to estimate the magnitude of flood that might have been required to enlarge the constrictions to the value of 0.5 observed for most debris fans (Fig. 6). A flood of 11,000 m^3/s (400,000 cfs) is estimated[16]. This is not an unreasonable estimate, because it is known that a flood of 8,500 m^3/s (300,000 cfs) occurred in 1884.

The calculations also indicate that when constrictions of the Grand Canyon debris fans reach the value of 0.45, the flow will be essentially subcritical[19] at all discharges. Although some standing waves and local regions of supercritical flow exist in most of the rapids of the Grand Canyon because of smaller-scale changes in bed elevation (including large rocks) than are considered in this simple model, the wave at Crystal Rapids was unique: other rapids that are less tightly constricted do not have strong normal waves (river rafters might disagree, because many of the existing waves are strong enough to flip rafts, but, at the scale of convergent-divergent constrictions considered here, these are local features.)

Over geologic time, the flow in Crystal Rapids can change from subcritical to supercritical (or vice versa) in two ways: (1) *as discharge changes* from season to season in a channel of fixed constriction, flow may pass from subcritical to supercritical, or vice versa; or (2) *as channel constriction changes* with time because of erosion during large floods or because of tributary debris flows. This evolution is summarized in Fig. 13, a version of Fig. 2 appropriate to Crystal Rapids that shows explicitly the response of channel shape and flow structures to changes in discharge. The sequence shown represents but one cycle in recurring episodes in which debris fans are enlarged by floods in the tributaries and then modified by floods in the main channel.

The beginning of the sequence is arbitrarily chosen as a time when the main channel is relatively unconstricted (Fig. 13a). The river is suddenly disrupted and ponded by catastrophic debris-fan emplacement (Fig. 13b), forming a "lake" behind the debris dam. The surface over which water pours across the freshly emplaced debris fan is called a "waterfall" in this model. As the ponded water overtops the debris dam, it erodes a channel, generally in the distal end of the debris fan (Fig. 13c). This is the beginning of evolution of a "rapid" from a "waterfall." Observations of naturally emplaced earth dams suggest that the breaching of the Crystal debris dam probably happened within hours or days of its emplacement.

Unless the debris dam is massively breached by the first breakthrough of ponded water (that is, unless enough material is removed so that the shape parameter is initially greater than 0.5), the constriction of the river is initially severe. Floods of differing sizes and frequency erode the channel to progressively greater widths (Figs. 13c, 13d, and 13e). Small floods enlarge the channel slightly, but constricted, supercritical flow is still present (e.g., as in Crystal Rapids from 1966 to 1983). Moderate floods enlarge the channel further, and the geometry observed at any instant reflects the largest flood in the history of the fan. Rocks from the debris fan are transported as far as 1 km downstream by the high-velocity water in the convergent, constricted, and divergent regions to form the "rock gardens" that lie below many such debris fans (Fig. 5a shows the Crystal rock garden).

Mature debris fans that once blocked the Colorado River and now have channels cut through them have progressed with time from the bottom to the top of Fig. 2 (or,

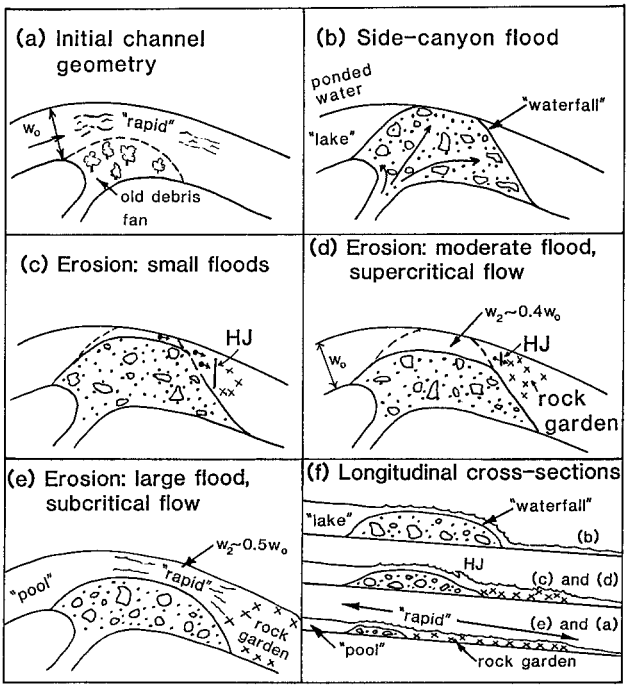

FIG. 13. Schematic illustration of emplacement and modification of debris fans in the Grand Canyon, modeled after the processes observed at Crystal Rapids during 1966-1983. HJ indicates a hydraulic jump. See the text for a discussion of (a)-(e). (f) Schematic longitudinal cross sections through the main channel in (a)-(e).

cyclically, from Fig. 13a to 13e), because natural floods have been large enough to create subcritical channels from the initially supercritical constrictions. Controlled discharges through Glen Canyon Dam will not permit Crystal Rapids to evolve to the configuration of the older debris fans. It is awesome to realize, however, that the controlled releases from the dam (2,600 m^3/s (92,000 cfs)) are sufficient to significantly alter the channel of the river should it become blocked or tightly constricted by tributary floods in the future.

What perspective does this interpretation of the history of the hydraulics and geomorphology of the Colorado River give us on the role of fluid mechanics in geology? First, the interpretation of a major wave as a hydraulic jump arising not from a rock but from large-scale channel geometry provides a different perspective for monitoring and predicting events at newly formed rapids -- a perspective valuable for National Park Service officials concerned with navigational safety. Any rapid newly formed by a debris flow may exhibit hydraulic features different from those seen in channels through older debris fans, because of the severe constriction that can be present. These rapids should be monitored closely if unusually high discharges are put through Glen Canyon Dam.

Second, the interpretation of critical flow in the constriction and supercritical flow downstream from the constriction predicts erosion in quite different places than would be found in a subcritical nozzle, and the interpretation of this shape allows modeling of sizes of ancient floods. Interpretation of the flow in this way also allows a mechanism for transporting large boulders a significant distance downstream from the original debris deposit into rock gardens, because of the high velocities that can occur downstream of the constriction in supercritical flow. Without such a mechanism, geologists are faced with the dilemma that tributary debris flows from side canyons are building weirs across the canyon, and downcutting through these weirs is difficult because only local abrasion or chemical solution can be invoked to get rid of the rocks. The relative roles of local abrasion, solution, and downstream transport of large particles must be understood before quantitative models of infilling versus downcutting of the Grand Canyon can be formulated.

Finally, the framework of supercritical to subcritical evolution of the rapids with time and through flood events of different sizes suggests new directions for geologic and hydraulic observations at the rapids: searches for geologic evidence of the estimated 8,500 m^3/s (400,000 cfs) prehistoric flood; evaluation of the relative roles of lateral constriction versus vertical topography on the channel bottom; documentation of wave behavior as discharge changes; laboratory experiments on the three-dimensional shapes of hydraulic jumps in flumes of converging-diverging geometry; development of criteria for transport of large boulders (>1 m) by fluids (a research topic that will be discussed again in the concluding section of this paper on the Mount St. Helens lateral blast); and evaluation of the relative frequencies of tributary versus main stem floods in determining the rate of downcutting by the Colorado River within the Grand Canyon.

IV. Old Faithful geyser: a two-phase nozzle

A. Geologic setting

Reports of geysers and hot springs in the land that is Yellowstone National Park began in the early part of the 19th century. Old Faithful Geyser has since become a familiar symbol of the western lands of the United States and their national parks (Fig. 14). More recently, Old Faithful became an important focus of scientific studies when striking resemblances between a peculiar type of volcanic seismicity known as "harmonic tremor" and the seismicity of the geyser were noted and explained[20] (Fig. 15). Harmonic tremor is a relatively monochromatic seismic motion that often precedes or follows volcanic eruptions; as a precursor, it has been invaluable in forecasting eruptions, even though no theory has adequately explained its origin. Harmonic tremor is also an important component of the seismic noise characteristic of geothermal fields, and it is thus potentially an important prospecting tool for geothermal energy sources -- sources that may provide only a few percent of the total energy requirements of the United States, but that could provide a substantial and critical portion of the energy

FIG. 14. Old Faithful geyser, Yellowstone National Park, in eruption. The column is about 30 m high. Note the discrete elements of fluid in the eruption column. These are the "surges" referred to in the text. Photo by G. Mendoza.

requirements of many countries surrounding the Pacific Basin. In this section, I summarize my observations and theory for the origin of harmonic tremor at Old Faithful, the importance of fluid properties in interpretation of the data, and my ideas about the complex process that occurs when the geyser erupts.

For perspective, fluid dynamicists might imagine Old Faithful as a vertical, open-ended, two-phase shock tube with variable cross section. In addition to the compressibility effects that normally dominate shock-tube dynamics, gravitational (hydrostatic) effects strongly influence the fluid properties in the geyser, because each meter of liquid water (providing approximately 0.1 bar pressure) changes the boiling temperature of the fluid by about 2 °C. Thus, in contrast to a shock tube in which initial conditions are usually isothermal and isobaric, the initial pressure and temperature conditions in Old Faithful are not uniform. The recharge cycle of the geyser is analogous to the process of filling a shock-tube driver section with a volatile liquid -- such as liquid Freon -- that can boil upon decompression, except that there is no physical diaphragm to contain the fluid; the natural diaphragm is the highest water in the conduit that maintains a temperature of 93 °C (the boiling temperature at the 2200-m elevation of Old Faithful) and sufficient pressure to keep deeper water from massive boiling and eruption. And

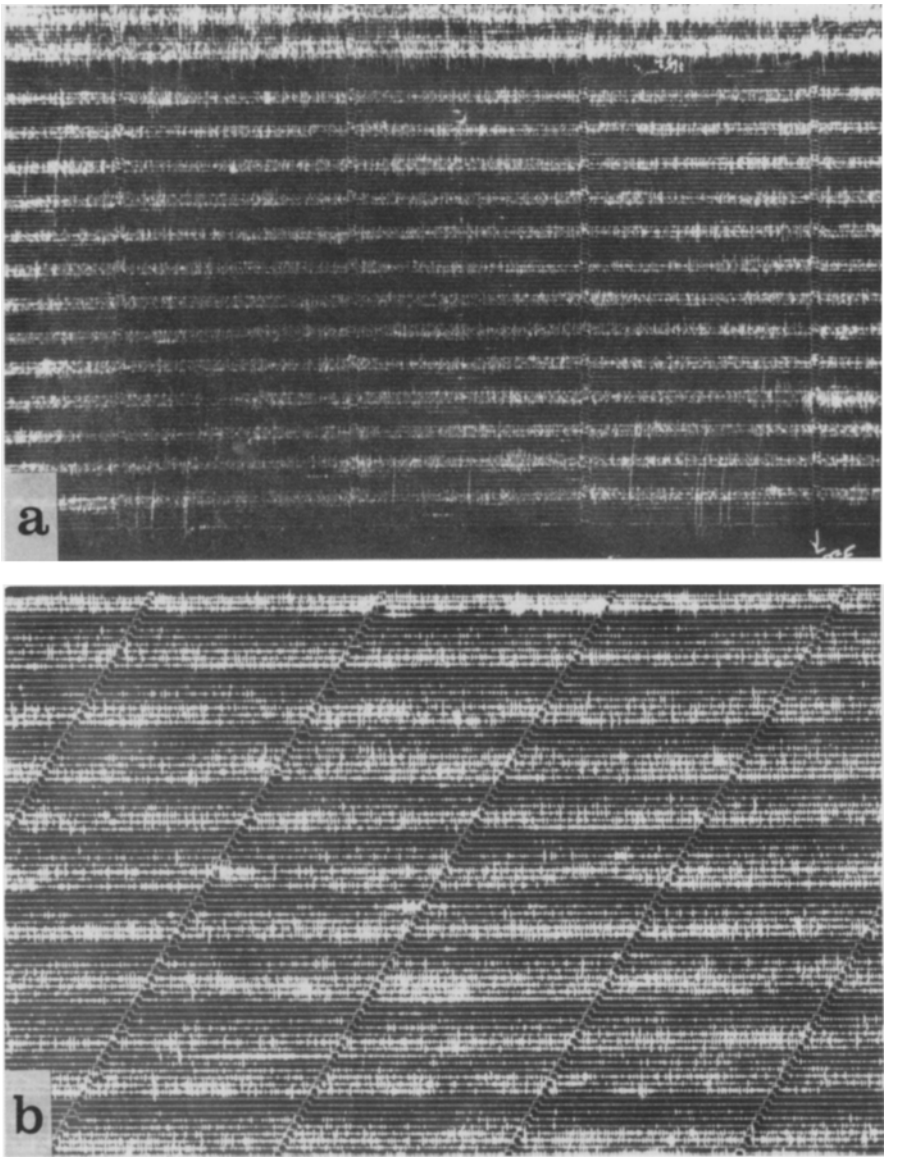

FIG. 15. (a) A seismic record from Karkar volcano, Papua New Guinea (courtesy of C. McKee and R.W. Johnson[21]). The white bands are strong seismic activity at a frequency of 2-4 Hz that recurs at intervals of about 70 minutes. (b) A seismic record of about one day of eruptions at Old Faithful, showing 11 complete eruption cycles (a higher-resolution record of one complete eruption cycle is shown in Fig. 20). The seismometer that obtained this record was a few tens of meters from the vent. Note the similarity to the Karkar record. The time marks in both records indicate 1-minute intervals. Each active period of the seismicity of Old Faithful ends with an eruption and a characteristic eruption coda; a good example of an eruption coda is on line 11,

beginning between the first and second time marks and extending to the fourth. A similar coda at the end of the active times on the Karkar record suggested to McKee and Johnson that underground eruptions were occurring at Karkar.

whereas in laboratory shock-tube experiments we worry about the "cleanliness" of eruption initiation over time scales of micro- to milliseconds, at an eruption of Old Faithful we may be lucky to forecast the initiation time to within 10 minutes!

Study of this complex shock tube must be done under very restricted conditions. Whereas a major problem in the study of the Colorado River discussed in the preceding section is inaccessibility, an equally major problem in studying Old Faithful geyser is its accessibility and public visibility. Observations close to the vent must be made on the few days of the year when work will not detract from tourists' enjoyment of the geyser (namely, when Yellowstone Park is closed for snow-plowing of the roads in late winter), and experiments or observations must be designed to avoid even the slightest damage to the geyser (for example, no hole can be dug to allow positioning and anchoring of a seismometer). Thus, the challenge in studying Old Faithful is to learn as much as possible about the inner workings of a complex nozzle from very limited observations. The basic data set consists of float and thermocouple measurements[22] made in 1949, seismic and movie data[20] taken from 1976 to 1984, and unpublished pressure and temperature data[23] that J. Westphal and I obtained in 1983 and 1984.

B. The recharge and eruption cycle

Old Faithful erupts into a tall, continuous vertical jet of water and steam (Fig. 14). The maximum height of the geyser ranges between 30 and 50 m, depending mostly on wind velocity and, to a certain extent, humidity (which affects the visibility of vapor in the eruption). Eruptions last for 1.5 to 5.5 minutes and occur every 40 to 100 minutes (Fig. 16). Measurements of total discharge suggest that about 0.114 m^3/s (114 kg/s; 1800 gal/min) are erupted during the initial and steady-flow stages of the eruption (E. Robertson, U.S. Geological Survey, private communication, 1977).

The conduit of the geyser, or the nozzle, is a fissure that is flared at the surface, narrows to a constriction at about 3 m depth, and probably diverges into one or more caverns below this depth (Fig. 17). About 0.5 m below the rim of the geyser, the fissure is 1.52 × 0.58 m, and I will take these as the dimensions of the exit plane of the fluid because the actual geyserite surface is very irregular (including a petrified tree stump visible as the knob on the left side of the cone in Fig. 14). Probe work by J. Westphal, R. Hutchinson and me (unpublished data) suggests that the constriction dimensions are approximately 0.1 × 1.5 m. The depth of the conduit that can be reached by a probe, the *immediate reservoir*, is 22 m, although it is plausible that water from greater depths is ejected during a long eruption. Water fills the conduit only to within 6 m of the surface

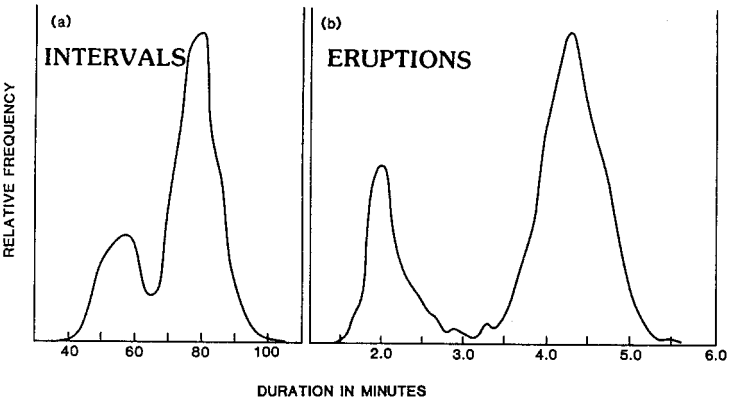

FIG. 16. (a) The relative frequency of intervals between eruptions of Old Faithful. (b) The relative frequency of eruptions of various durations. All data are for the year 1979; the vertical scale is arbitrary. Unpublished data provided by R. Hutchinson, U.S. National Park Service, from analysis of 3,308 eruptions, 1983.

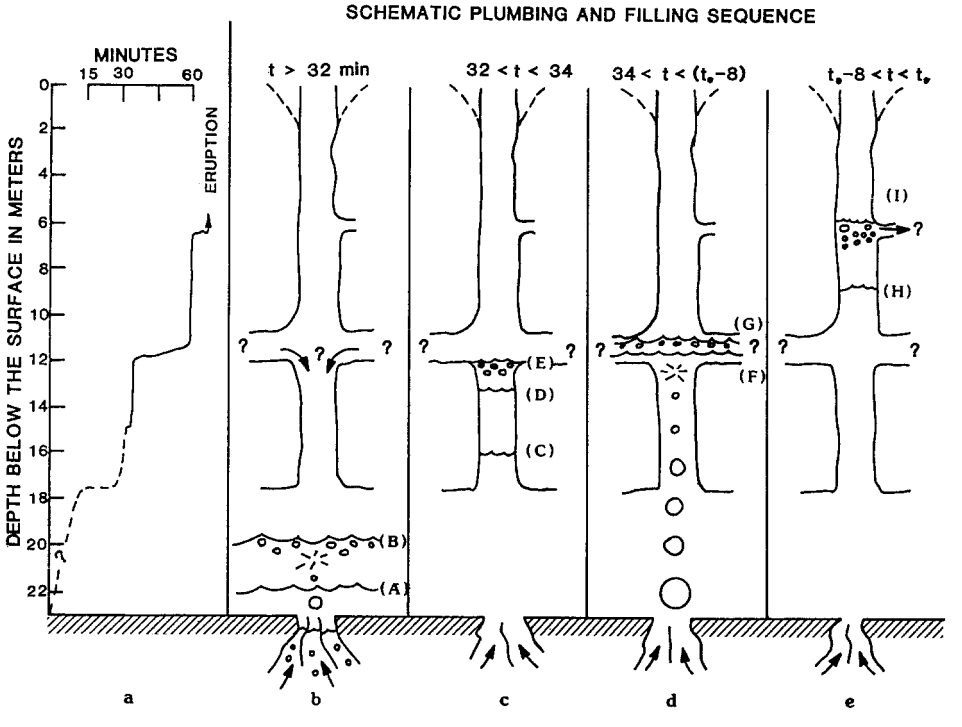

FIG. 17. (a) Rate of filling of Old Faithful, as inferred from float measurements reported in 1948[22]; time = 0 was taken when probe was lowered. Recent work by Kieffer and J. Westphal (unpublished) shows differences in details of the filling rate but does not change the general discussion chosen for this paper. (b)-(d) Schematic diagram of the conduit of Old Faithful, based on the float measurements and an assumed

constant rate of recharge. The time until the next eruption is indicated at the top. The important points to note from these sketches are (1) the gradual recharge of water over the interval prior to eruption (the levels A-I represent inferred depths of the surface water at different times); (2) the addition of heat via hot water and/or steam bubbles at the base of the recharging column; and (3) continuous boiling of the near-surface water. Collapse of steam bubbles within the liquid zone is inferred to be the cause of seismicity.

(Fig. 17). The maximum length of the water column in the immediate reservoir prior to an eruption is therefore about 16 m.

For nearly a century after its discovery, Old Faithful maintained a fairly regular pattern of eruptions, with intervals between eruptions averaging 60 to 65 minutes. During most years, Old Faithful exhibited two types of eruptions: "shorts," which were 2.5-3.5 minutes in duration, and "longs," which were about 5 minutes in duration. During the 1970's, the length of the repose interval, I, following an eruption was quite closely related to the duration of the eruption, D. The empirical formula

$$I = 10\,D + 30 \qquad (I, D \text{ in minutes}) \tag{17}$$

proved very useful to the National Park Service for predicting when eruptions would occur.

In the past few years the duration-interval behavior has changed dramatically, although changes in the observable eruption characteristics of the geyser during an eruption (such as height versus time) have not been documented. Intervals averaged over a month commonly exceed 75 minutes and individual intervals have sometimes exceeded 100 minutes. The interval-duration equation no longer applies to the same statistical accuracy; in 1987, short eruptions ceased for a while, and only long eruptions occurred (R. Hutchinson, National Park Service, private commununication, 1987). The mysteries of geyser eruptions have long intrigued scientists (the original theory of the inner workings of geysers was published by Bunsen in 1846), but questions about the inner workings of Old Faithful have taken on a new urgency because of these dramatic changes in behavior.

C. The recharge process: clues to geothermal seismicity

After an eruption ceases, the conduit is empty (or nearly so) and must be recharged with both water and heat. Estimates of total volume erupted and conduit dimensions give an approximate recharge rate of 6 kg/s (liquid water) (see Ref. 20, p. 66). A working model for recharge of fluids and heat to the geyser is based on measurements of depth and temperature versus time[22]. Water rises slowly up the conduit during the recharge interval (Fig. 17). During the rise, temperatures range from 93 °C at the

surface to 116 °C-118 °C at the bottom of the immediate reservoir (Fig. 18, temperature-depth-time curves). The hottest water at the bottom is about 7-9 °C below the boiling temperature for the total pressure at the bottom (0.08 Mpa (0.8 bars) atmospheric pressure + 0.14 Mpa (1.4 bars) hydrostatic pressure). Because the deep water is hotter than the shallow water, heat for the recharge cycle is most likely supplied by the addition of hot water or steam at the base of the immediate reservoir.

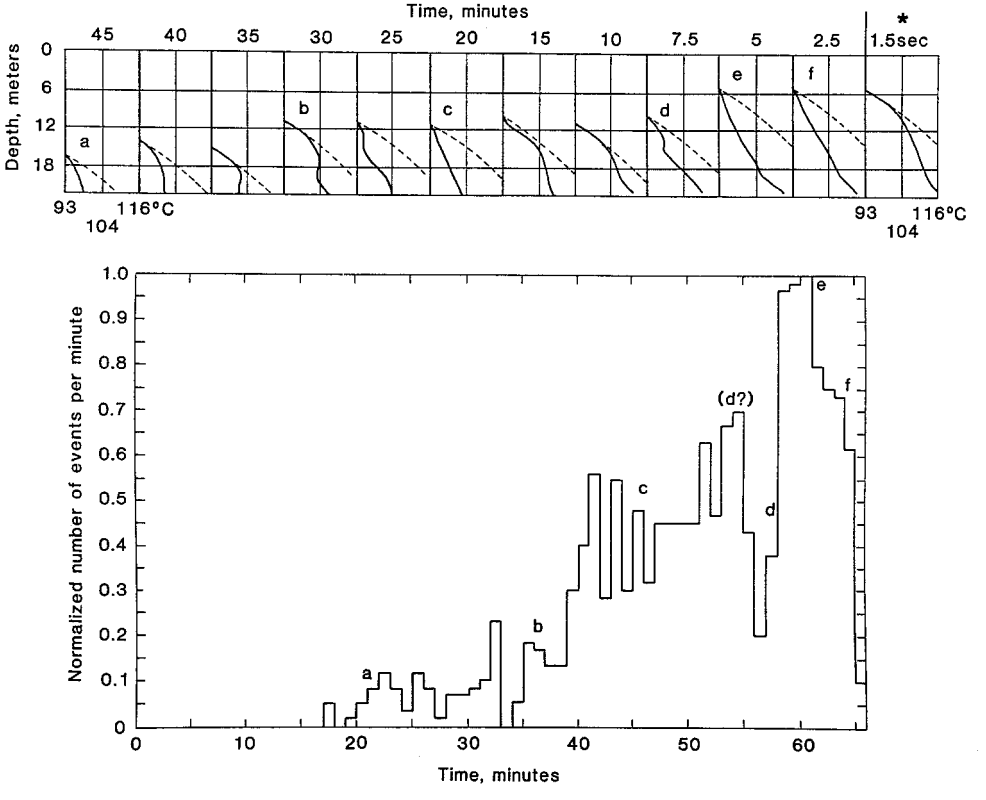

FIG. 18. A histogram of the number of seismic events per minute through a recharge interval at Old Faithful, supplemented by data on the depth of water in the conduit at various times (the graphs above the histogram) and the temperature of the water relative to the reference boiling curve (the top curve in each graph). The temperature-depth data were not taken during the same eruption as the seismic data; for details of the construction of the correlations shown here, see Kieffer[20]. On the bottom axis, time = 0 is taken at the beginning of an eruption that was about 4.5 minutes long; a 66-minute interval followed before the next eruption. The first appreciable seismicity starts at about 21 minutes (45 minutes before the next eruption), and the associated temperature-depth conditions are indicated by the left box labeled "45 min." Successive graphs labeled with decreasing times (40, 35, 30 min, . . . to 1.5 sec) show the gradual filling and heating of the geyser and the correlations with seismic details.

Two processes probably contribute to the mixing of the hot deep water with the cooler surface water: convection and migration of steam bubbles. It is not clear that the two processes can be distinguished using available measurements (note the erratic temperatures at any fixed depth; e.g., at 18 m in Fig. 18). Much of the deeper water is too cool to boil under the total pressure (hydrostatic + atmospheric) at any given time; compare the measured temperatures with the reference boiling curve given in each box in Fig. 18. However, since the temperature of the deeper water exceeds the atmospheric boiling temperature of 93 °C, this water is superheated relative to the boiling point at atmospheric pressure. If such superheated water is convected upward, steam bubbles form as the pressure decreases below the saturation pressure of the water. For example, 3 percent of the deep water at 116 °C will transform to steam when the total pressure decreases to 0.1 Mpa (1.0 bar). As steam bubbles rise, however, they encounter cooler water and may collapse. Although this process cannot be directly observed in the depths of Old Faithful, it is easily observed in a pot on a stove, as well as in other geysers, such as Strokker in Iceland, where the steam bubbles rise into a diverging surface pool and can be observed both to collapse before reaching the surface, and to reach the surface and explode into a beautiful fragmenting shell (Fig. 19). In geysers where the bubbles can be directly observed, they frequently occupy the full diameter of the conduit, which may be of the order of, or more than, 1 m. Collapse of the bubbles, and release of their latent heat, is probably a major process by which heat is transferred upward in the water column[24], and the collapse of these bubbles is believed to cause the individual seismic events observed.

The collapse of a vapor bubble in a liquid of its own composition can occur within milliseconds[25], and pressures in the collapsing cavity can be as large as a few to tens of

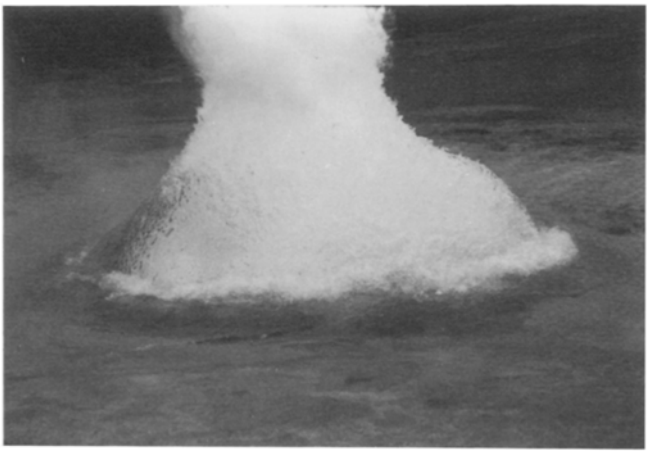

FIG. 19. Bubble erupting from the vent of Strökkur geyser, Iceland, through a surface pool of water. The bubble diameter is about 2 m. Note the fine-scale structure on the bubble surface. Photo by H. Kieffer.

megapascals (tens to hundreds of bars)[25,26]. The high pressures generated by the bubble collapse decay quickly with distance, becoming seismic-level disturbances at distances of only a few bubble radii.

The acoustic noise of collapsing steam bubbles can be detected by seismometers placed around Old Faithful (Figs. 15a and 20). The seismic codas of two eruptions, labeled A and B, are shown in Fig. 20. These codas are primarily due to water falling back from the top of the erupting column onto the ground (this fallback was just beginning to occur when Fig. 14 was taken; it is visible on the right side of the photograph). Short, discrete bursts of seismicity occur throughout most of the recharge interval (four such events, indicated in Fig. 20, are shown enlarged in Fig. 21). The number of seismic events per minute increases as the geyser fills and the fluid becomes generally hotter (Fig. 18, histogram).

Two characteristics of this seismicity are the relatively high frequency content of the individual events (a few tens of Hz) and the characteristic damping time of a few tenths of a second. The envelope of these signals is remarkably similar in shape to those obtained by Hentschel[27] in laboratory experiments on collapsing bubbles, although the geyser signals are much longer in duration (tenths of seconds compared with hundreds of microseconds), presumably because of the much larger size of the geyser bubbles.

A collapsing bubble could cause the observed seismicity by generating waves within the fluid column, as illustrated in Figs. 22a and 22b. These waves set the fluid in the conduit into resonance; that is, the conduit is an organ pipe filled with liquid water and is set into resonance by the occasional (or frequent) collapse of a large steam bubble. Detailed treatment of the disturbance caused by a single bubble as a hydraulic transient[20] accounts for the distensibility of the conduit walls and allows the damping of the signals to be calculated. To first order, the frequency of the oscillation induced is assumed to be that of a closed organ pipe:

$$f = a/4L \ , \tag{18}$$

where L is the length of the fluid column in the conduit, and, in this equation, the sound speed, a, is the effective sound speed of the fluid modified for the distensibility of the conduit walls[28]. Whereas a is 1,440 m/s for pure water, it decreases to 1,385 m/s if the distensibility of the walls of the conduit is accounted for.

The length of the fluid column in the conduit, L, depends on the time in the recharge cycle (note in Figs. 17 and 18 how slowly the recharge process occurs): L is estimated to be 8 m when the seismicity is first detected and 16 m when the conduit is full near the time of an eruption (Figs. 17c-17e and Fig. 18). The corresponding resonant frequencies obtained from Eq. (18) are 43 and 20 Hz, values that approximately span the range of measured frequencies during the recharge interval (Fig. 21). From hydraulic transient theory, the characteristic damping time is 0.12 to 0.46 s, in good agreement with the duration of the observed pulses (Fig. 21).

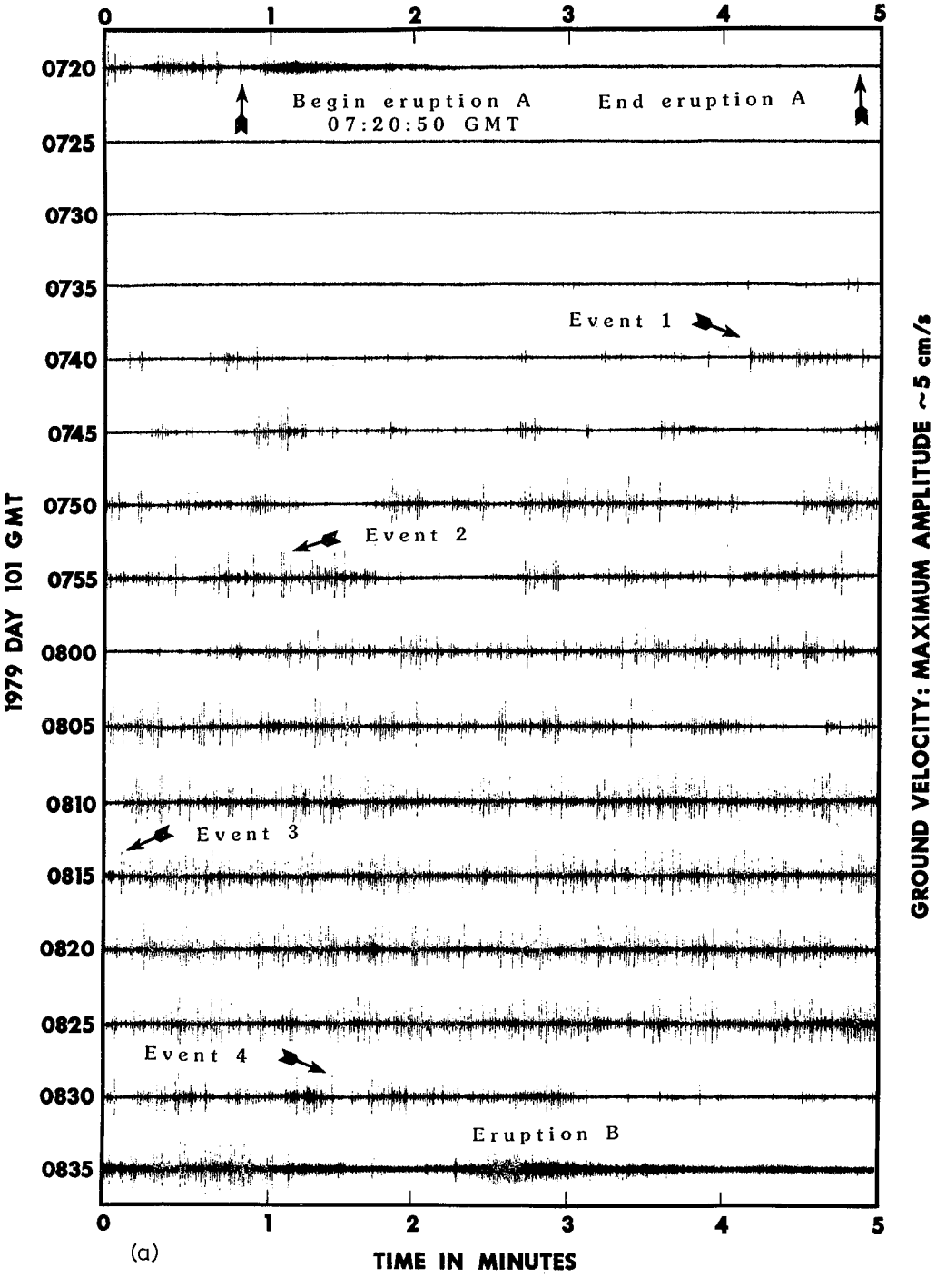

FIG. 20. A seismic record of one eruption cycle of Old Faithful. Details of the four seismic events labeled 1-4 are shown in Fig. 21. To obtain the histogram of Fig. 18, the number of these events exceeding a peak-to-peak amplitude of 4 cm per second was counted.

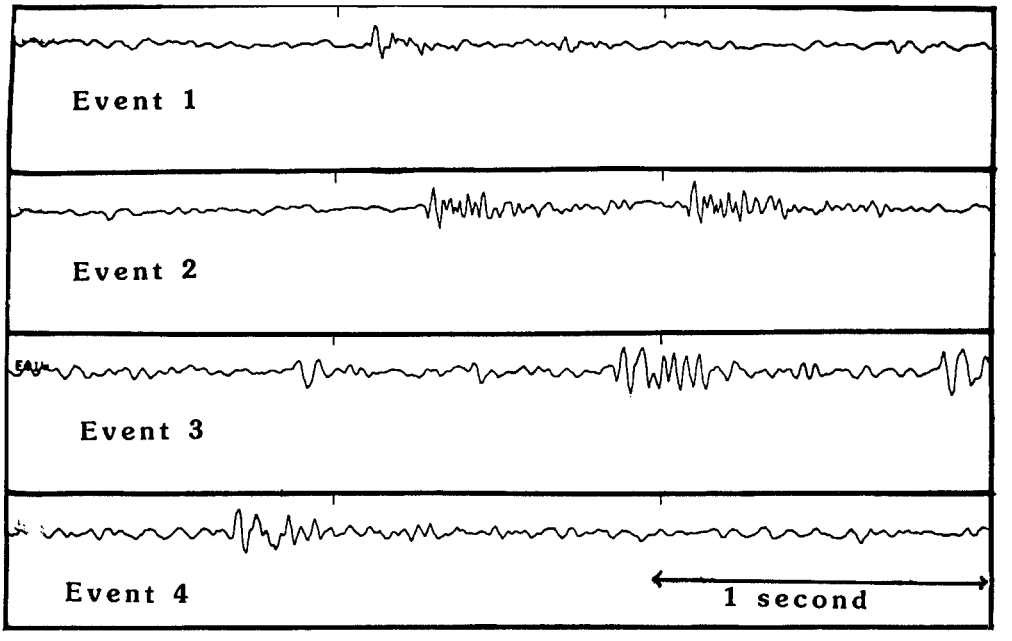

FIG. 21. Details of four impulsive seismic events from Old Faithful as indicated in Fig. 20. Note that the dominant frequencies range from ~ 20 to ~ 40 Hz.

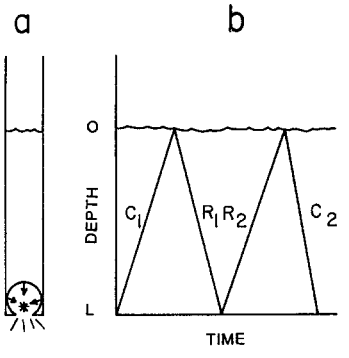

FIG. 22. Schematic drawing of waves propagating in a standing column of water of depth L. (a) The collapse of a steam bubble in the base of the column is indicated by an asterisk. (b) One cycle of compression (C) and rarefaction (R) waves due to bubble collapse in the bottom of the conduit.

The resonant frequency associated with individual seismic events, and the duration of each event during the pre-eruption seismicity at Old Faithful, can be explained, to first order, as arising from hydraulic transients in a slowly recharging column of *liquid* water. If the fluid in the conduit were, for example, a boiling, two-phase mixture, the sound speed would be dramatically lower, and the observed seismicity could not be

explained so simply as arising from resonances of the liquid column standing in the immediate reservoir. In the next section, I describe the thermodynamics of the transformation of the recharged liquid in the conduit as an eruption occurs, and show how the associated change in sound speed of the fluid influences the resonant frequencies of the conduit.

D. Eruption dynamics and thermodynamics

An "eruption cycle" of Old Faithful consists of one eruption and one recharge interval. By convention, the start of an eruption cycle is taken as the onset of an eruption, although the first part of an eruption actually begins below ground level and cannot be monitored (see the discussion of preplay below). The visible flow field and its variation with time during an eruption are collectively referred to as the "play" of the geyser. The play consists of four parts which can be distinguished on a graph showing the height of the eruption column versus time (Fig. 23).

The first part of an eruption (the part that begins underground) is *preplay*, the ejection of water intermittently prior to the actual eruption (the last few episodes of preplay before the eruption, from −15 s to 0 s, are shown in Fig. 23). Episodes of preplay last for a few seconds, and water is thrown to a height of a few meters or occasionally a few tens of meters. During preplay, water ejected upward into the atmosphere is cooled by expansion and entrainment. When it falls back into the conduit, it mixes with the heated conduit fluid, and the resulting cooling of near-surface water can delay the onset of an eruption until the fluid has been reheated to initiation conditions.

During *initiation and unsteady flow* the eruption column develops and rises in a series of *bursts* (typically 1 to 8 in number) to a maximum height of about 30 m to 50 m. This part of the eruption is typically 20 to 40 s long. Two minor bursts and four major ones occurred during the first 20 s of the eruption documented in Fig. 23.

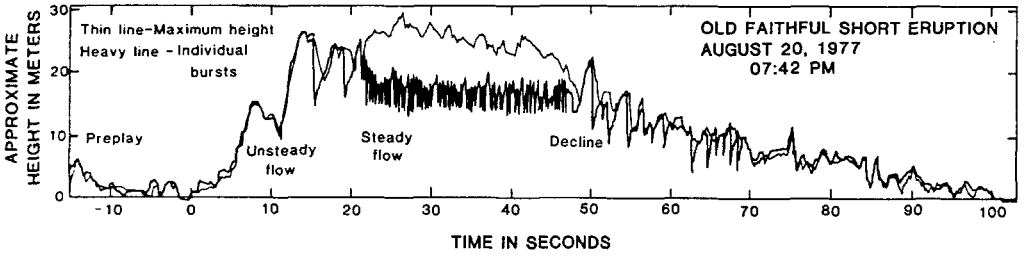

FIG. 23. A record of height versus time for a short eruption of Old Faithful, showing the four stages of eruption discussed in the text. The light line is the height of the water-steam column; the heavier line traces individual pulses of water, visible in Fig. 14, in order to obtain the frequency of surging (approximately 1-2 Hz).

Steady flow is an interval of about 30 s during which the column stays near maximum height. During this time, *surges* are observed in the eruption column at a frequency of about 2 Hz in short eruptions and 1-1.5 Hz in long eruptions (Fig. 24b). The surges are shown photographically in Fig. 14, and graphically from 20 to 45 s of the eruption documented in Fig. 23.

The *declining part of the eruption* begins rather dramatically, after roughly 30 s of steady flow, with a drop in column height. The decline can last up to 3 min, and during this time the height of the column drops to about 10 m and play continues at low levels.

Differences between long and short eruptions are threefold: the frequency of surging during the steady-flow stage; the duration of the decline stage; and the seismic pattern following the eruption. Analysis of height-time data (such as shown in Fig. 23) for many eruptions reveals that there is no correlation of maximum height obtained, duration of maximum height, or number of bursts in the initiation stage with eruption duration (Fig. 24a). The only measurable differences in eruption play between long and short eruptions are the frequency of the surges (Fig. 24b) and the duration of the decline phase, which is simply truncated at about 2-3 min for a short eruption. Seismically, a period of about 20 min of quiet follows a long eruption (Fig. 20), whereas seismicity begins immediately after a short eruption. After short eruptions, we are able to hear water splashing in the bottom of the immediate reservoir, which suggests that it is not completely emptied during short eruptions and that the seismicity arises within the immediate reservoir.

Water near the surface of the recharging column boils nearly continuously, and vigorous boiling can accelerate fluid several meters upward. Early in the recharge cycle, the fluid is too deep in the conduit for vigorously boiled water to be ejected over

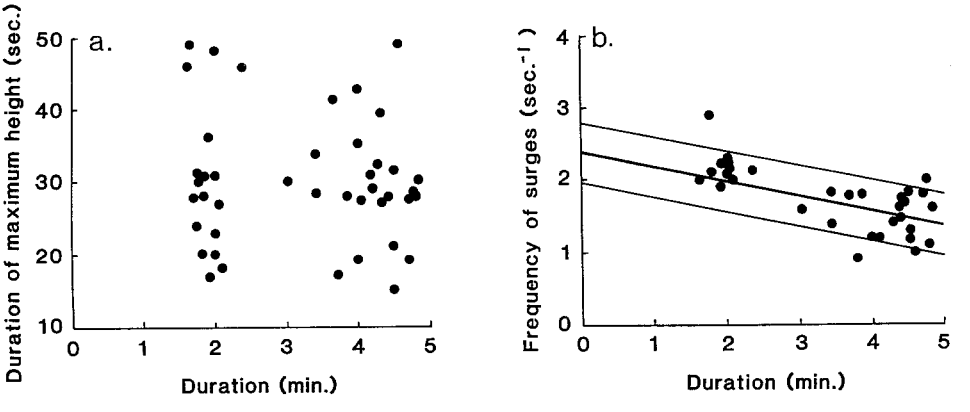

FIG. 24. (a) Graph of duration of steady-flow stage (maximum height) versus duration of eruption of Old Faithful geyser, showing no correlation. (b) Graph of frequency of surges versus duration of eruption, showing inverse correlation.

the rim. Thus, even though vigorous boiling and splashing occur within the conduit, the pressure distribution at depth remains unchanged because fluid is not removed from the conduit and an eruption cannot begin. An eruption therefore begins when two criteria are met: (1) the water must have risen high enough in the conduit so that vigorous boiling can discharge some water over the rim, thereby reducing the hydrostatic pressure on the fluid by removal of some mass; and (2) the underlying water must be hot enough that the mass unloading triggers a positive feedback process.

As the recharging fluid rises to within about 6 m from the top of the conduit, boiling can eject fluid out onto the cone of the geyser. This removal of mass reduces the pressure on the underlying fluid. If the underlying water is sufficiently close to the boiling curve, and if enough water is removed to start the cascading process of decompression, the unloading results in a positive feedback process whereby more boiling, and hence an eruption, occurs. If the underlying fluid is not sufficiently close to the boiling curve -- e.g., if relatively cool surface water has been recently overturned by convection -- the unloading may simply result in a burst of preplay and no eruption.

A simplified diagram of Old Faithful modeled as a layered shock tube is shown in Fig. 25, so that the words "enough" and "sufficiently close" in the above paragraph can be semiquantitatively defined. In the example shown, I have arbitrarily divided the fluid in the column into six cells of different, but uniform, temperature (cells B, C, D, E, F, G); these might be thought of as simplified convection cells. These cells mimic the temperature curve measured by Birch and Kennedy[22] 15 s before the onset of an eruption (Fig. 18, last temperature-depth graph). The top zone, A, 1 m in length, has been assumed to be continuously boiling and to be the mass of water that is ejected out of the conduit to start the eruption (Fig. 25a). I chose the length of 1 m for this zone somewhat arbitrarily after watching the onset of about 200 eruptions and estimating the amount of water ejected.

When A is ejected out of the conduit, the pressure on the underlying water is everywhere reduced by the weight of the ejected fluid (assume this to be about 0.1 bar; SI units are abandoned temporarily here for ease in following Fig. 25). Relative to the reference boiling curve, therefore, the initial temperature distribution curve is elevated toward the boiling curve by 0.1 bar. If it is assumed that no large-scale temperature inversion exists (such as J, Fig. 25), some underlying water is now superheated with respect to the boiling temperature at the new pressure; specifically, any water that was originally within 0.1 bar of the reference boiling curve. In the example shown, the water between B and B′ will boil (Fig. 25b). When this water is erupted, more underlying water will boil: any water that was originally within 0.2 bar of the reference boiling curve. In Fig. 25, this is only the water between B′ and B″, although the water at the top of cell C is now very close to the reference boiling curve (Fig. 25c). When this water has been unloaded, the pressure is everywhere 0.3 bar less than the initial pressure, and water between B″ and B‴, as well as between C and C′, will boil. Note

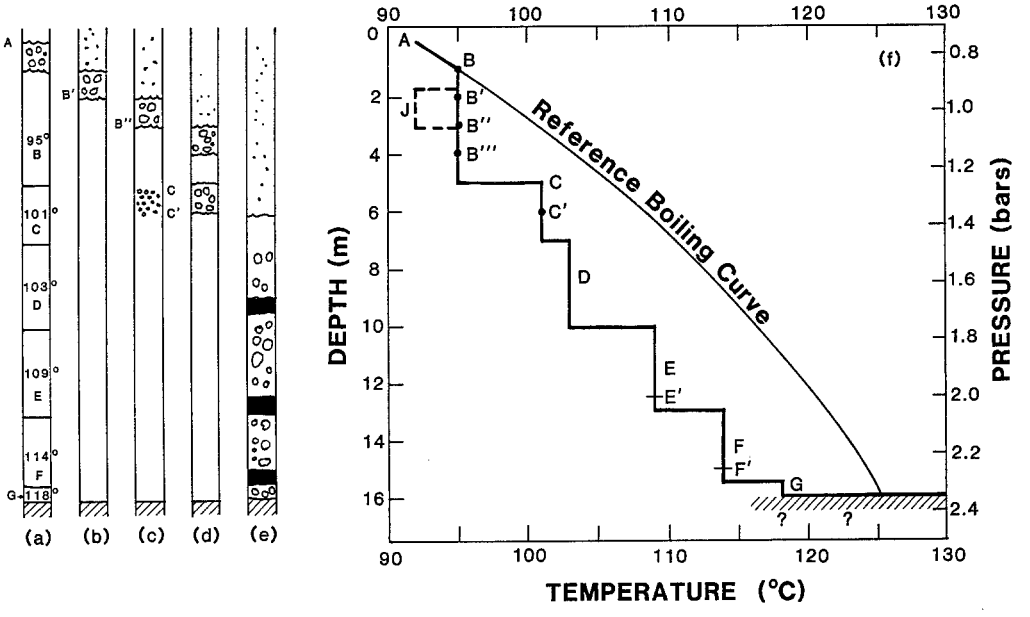

FIG. 25. Old Faithful modeled as a shock tube containing layers of fluid at different initial pressures and temperatures, shown in their position relative to the reference boiling curve in the right figure, (f). In (f) the initial temperature is assumed constant within six convection cells (labeled B, C, D, E, F, and G). The fluid between A and B is assumed to be at pressure-temperature conditions on the boiling curve in order to trigger the eruption. (a)-(e) Five stages in the unsteady unloading process of an eruption of Old Faithful; release of each of the five convection cells would presumably correspond to a "burst" observed as the geyser evolves into steady flow (see Fig. 23). The segments shown with large "bubbles" are boiling; the segments shown as a fine "mist" are erupting from the conduit; and the three segments shaded black are liquid H_2O because of the relations of parts of cells D, E, and F to the reference boiling curve during the unloading process. The thermodynamic path of the unloading process is discussed in the text.

that, because of the weight of B″-B‴, the fluid between B‴ and C cannot boil until some of the fluid in B″-B‴ erupts from the conduit. Presumably, as the water between B″ and B‴ erupts, and as C-C′ boils and expands, the liquid water between B‴ and C will be pushed up and will boil as the pressure decreases. Slugs of liquid water trapped between slugs of boiling froth should be expected because of the different possible relations of the fluid temperature to the reference boiling curve (Figs. 25c-25e).

When fluid has been erupted down to level C′, 6 m of water will have been ejected, and the pressure in the column will be everywhere 0.6 bar less than the initial pressure. Except for small amounts of fluid between E′ and F and F′ and G (Fig. 25e), the fluid

will be everywhere on the reference boiling curve, and the conduit becomes nearly completely filled with a two-phase mixture. The fluid is probably a boiling liquid at depth, grading upward into the steamy aerosol that emerges at the surface.

Further details of this unloading process are unknown; depending on the constriction, shock and rarefaction waves may play a prominent role in ejecting the different layers of water[20], or choked flow may be more important in controlling the mass flux rate (see below). Resolution of this question may only arise from detailed theoretical or laboratory modeling, because of the extreme difficulty of field measurements of conduit geometry and time history of the fluid flow.

At the onset of an eruption, liquid water is present everywhere in the conduit except in the boiling zone at the surface. Boiling to progressively deeper levels decreases the amount of liquid present and replaces it with a two-phase mixture (Fig. 25). Because the initial pressure-temperature curve at the onset of an eruption lies no farther than 0.05 to 0.07 Mpa (0.5 to 0.7 bar) below the reference boiling curve, the whole column of fluid in the conduit lies on the reference boiling curve after unloading of only 5 to 7 m of the water. Thus, when about half of the vertical length of the water column has been unloaded, the pre-eruption "organ pipe" filled with liquid water has been transformed into a steamy two-phase nozzle. (Note that if the conduit is perceived as a nozzle, the original standing water only occupied 16 m of length, whereas the erupting fluid fills the full 22 m, and extends into a jet 30 to 50 m high outside the conduit.) It is likely that the "bursting" observed during the unsteady initiation of the eruption represents the eruption of progressively hotter parcels of water, and that the transition from unsteady bursting flow to steady surging flow observed in the behavior of the eruption column (Fig. 23) occurs when the whole immediate reservoir is filled with a two-phase fluid.

As the water in the base of the reservoir is decompressed to atmospheric pressure, some of the enthalpy stored in the hot fluid is converted to kinetic energy. The hottest water, at 116 °C, has an enthalpy (relative to the triple point) of 486.72 kj/kg and an entropy of 1.4842 kj/(kg·K). If this fluid decompresses isentropically to 93 °C, at 0.08 Mpa (0.8 bars) pressure, 4 percent of the liquid is converted to vapor. The final enthalpy of the mixture is 482.83 kj/kg, so 3.89 kj/kg are available for kinetic energy. This is sufficient energy to accelerate the fluid isentropically to a velocity of 88 m/s.

Although the velocity at the exit plane of the geyser has not been directly measured, a simple ballistic calculation of velocity based on the height of the eruption column can be used to estimate ejection velocity[20]. This calculation, using $x_m = u_o^2/2g$, where x_m is the maximum height, u_o is the exit velocity, and g is the acceleration of gravity, gives $u_o = 31$ m/s for $x_m = 50$ m. If the acceleration is presumed to begin at the base of the conduit, x_m could be about 70 m, and u_o from this model is 37 m/s. However, because an eruption of Old Faithful produces a jet rather than a "ballistic billiard ball", the simple ballistic equation may not accurately estimate the exit velocity. Experiments on the dynamics of negatively buoyant plumes[29] give the relation

$$x_m = 1.85\, F^{1/2} D \ , \tag{19}$$

where F is the densimetric Froude number:

$$F = u_o^2 \left[\frac{\rho_o}{(\rho_a - \rho_o)\, g\, D} \right] . \tag{20}$$

In this equation, ρ_o is the fluid density, ρ_a is the density of the fluid into which the jet is emerging, and D is the diameter of the jet, assumed axially symmetric. (This F is comparable to $(Fr)^2$, with Fr defined as in Eq. 15). The absolute value of the density difference is used in Eq. (19), where the square root of F is needed. For the exit plane at Old Faithful (1.5 m × 0.6 m fissure), take $D = 1.1$ m. Assume that $\rho_o = 11.23$ kg/m^3 (4 percent vapor) and $\rho_a = 0.7$ kg/m^3. The above equations then give $u_o = 78$ m/s, a value in surprisingly good agreement with the velocity of 88 m/s predicted simply from the enthalpy change of the fluid.

The low-frequency surging (~ 1-2 Hz) observed when the geyser is in steady flow (Figs. 14, 23, and 24) could be the resonances of the conduit filled with the two-phase mixture. The sound speed of an H_2O mixture that is 4 percent vapor is 57 m/s at 1 bar pressure and does not vary significantly between 0.8 bar atmospheric pressure and 0.18 Mpa (1.8 bars) vapor pressure for the fluid boiling at 116 °C at the bottom of the vent (the sound speed would decrease dramatically as the vapor fraction approaches zero, as shown in Fig. 3, vertical line (a), but I assume that the vertical range over which this occurs is small). The resonant frequency of a 22-m closed pipe with this sound speed would be 0.64 Hz, corresponding to a period of 1.5 s. This frequency is about a factor of 2 lower than that measured for a long eruption (1-1.5 Hz), but it probably must be considered in satisfactory agreement, given the simplicity of the model, the unknown geometry of the conduit, and the extreme difficulty of measuring each individual eruption surge.

Because we have no reason to believe that the sound speed of the fluid is any different in long versus short eruptions, the change in surge frequency with eruption duration can be interpreted as representing an effective change in the length L of the resonating column. The possibility that multiple chambers containing fluid exist cannot be excluded, and emptying of different numbers of such chambers could account for an effective change of L. Another possibility is that water is vaporized to different levels in the eruptions of differing durations. During a long eruption, for example, all water in the immediate reservoir is converted into a two-phase mixture, and the immediate reservoir is completely emptied (evidence for this consists of lack of any audible splashing within the reservoir for about 20 minutes after such an eruption, and lack of seismicity during this time). For the long eruptions, the bottom of the conduit is probably truly the geyserite bottom reached by probe, and L is the measured 22 m. During a short eruption, only part of the water in the immediate reservoir appears to be

discharged (as evidenced by audible splashing in the conduit immediately after such an eruption ceases, and concurrent resumption of seismicity). There is, therefore, probably a level below which water does not vaporize during short eruptions. In these eruptions, the surface of the unvaporized water would be the effective bottom of the reservoir, because of the large difference in acoustic impedance between boiling and liquid water; that is, the length L would not be the conduit length, but a shorter value equal to the length of water column vaporized. This could account for the higher surge frequencies observed during short eruptions (Fig. 24b). The mechanism whereby the water, which was at 116 °C at the beginning of the eruption, is prevented from vaporizing under pressure reduction remains a mystery. The most common speculation is that cold water can occasionally enter the reservoir during an eruption, but there is no proof of this.

E. Speculations and summary

Is the flow from Old Faithful choked? Is there supersonic flow anywhere in the eruption jet? There are too few data to permit firm conclusions. A few speculations can be offered, although calculation of choking conditions in two-phase flow is a notoriously difficult problem, even in well-designed pipes[30].

The highest vapor pressures in the reservoir will be generated as the hottest water boils -- 0.175 Mpa (1.75 bars) as the 116 °C water boils. Equilibrium expansion to atmospheric pressure of 0.08 Mpa (0.8 bars) produces a fluid that is about 4 percent vapor. Given a maximum reservoir pressure of 0.175 Mpa (1.75 bars), the choke pressure can be calculated from theoretical considerations to be about 0.13 Mpa (1.3 bars)[31]. Experimental evidence[32] suggests that this calculated choke pressure is too high and that the choke pressure could be as low as about 0.55 of the reservoir pressure, about 0.09 Mpa (0.9 bar). The near similarity of atmospheric and estimated choke pressure suggests that the flow could be choked when this hottest water is flowing, but that supersonic flow in the diverging part of the conduit will be weak. The discussion above of the decompression process suggests that choked flow would be most likely during the steady-flow stage, beginning 20 to 30 seconds into the eruption.

Assume that choking occurs at conditions very close to those seen at the exit plane; that is, at 0.1 Mpa (1 bar) pressure when the fluid is about 3 percent vapor. The mass flux is given by

$$\dot{m} = \rho A \, a^* , \tag{21}$$

where a^* is the sound speed, 45 m/s for equilibrium. The density of the fluid is 19.68 kg/m^3 (3 percent vapor), and the choke area is about 0.15 m^2. The calculated mass flux is 132 kg/s (2100 gal/min). This is satisfactorily close to the measured value (114 kg/s; 1800 gal/min), given the extreme difficulty of measuring the discharge accurately and the relatively large uncertainty of the choke area, A.

If, as calculated above, the exit-plane velocity is ~ 80 m/s, and the equilibrium sound speed at the exit plane is 57 m/s, the implied Mach number at the exit plane is ~ 1.5, barely supersonic within the uncertainties of the modeling. It is therefore not surprising that shock features such as Prandtl-Meyer expansion, visible shock waves, or noise originating from shocks within the plume are not observed at Old Faithful. In contrast, Beehive Geyser (Fig. 26a), which sits just a few hundred yards from Old Faithful and erupts too erratically to be monitored, sounds like a jet engine and, with a little imagination, can be envisioned to contain internal shock waves. These shocks are similar to those observed at weakly supersonic geothermal wellheads (Fig. 26b).

In summary, Old Faithful is a complex two-phase nozzle, possibly sonic or weakly supersonic, and certainly large enough in scale for both gravity and compressibility to

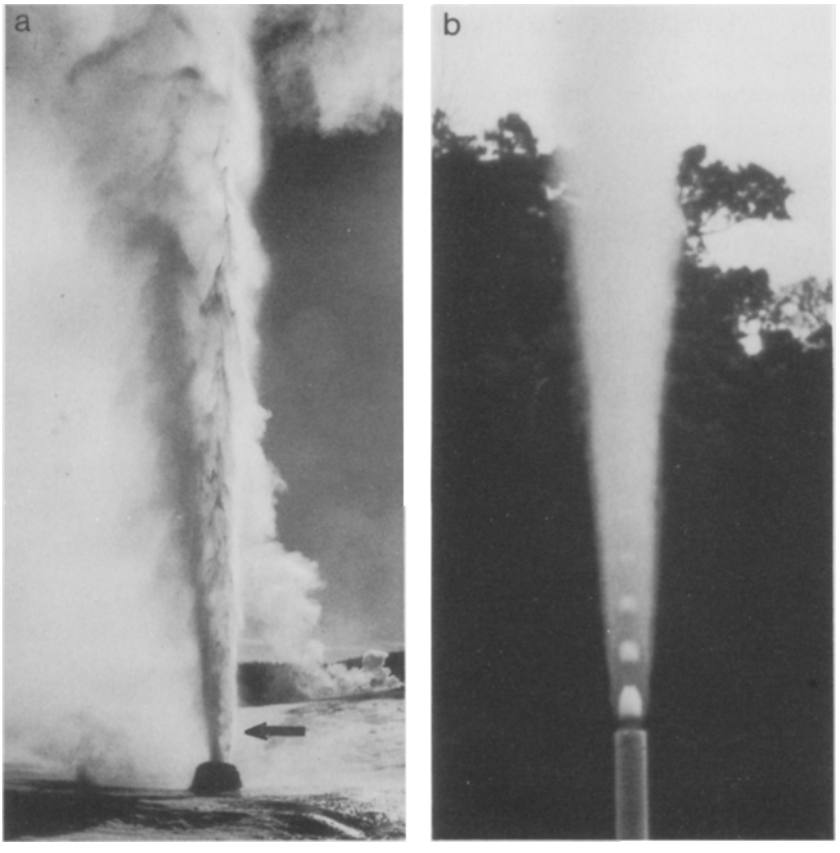

FIG. 26. (a) Beehive geyser in eruption; the cone is about 1 m high. The arrow points toward three white diamonds in the center of the flow, interpreted as shock-wave wave structures within a supersonic flow. Photo by Jeremy Schmidt[33]. (b) Photo of geothermal well MG-5, Tongonan, Philippines. Photo by Charles Darby, KRTA Ltd., Auckland, New Zealand.

be important. Although available data still do not permit a detailed model for the eruption dynamics, they have served to point out new directions for experiments and observations, some of which are now in progress. One of the most important directions of research focused on by these discoveries relates to the similarities in seismicity between geysers and volcanoes that exhibit harmonic tremor (Fig. 15). Harmonic tremor has for decades been attributed to magma motion in volcanoes, but the quantitative nature of the mechanism causing it has been elusive. The geyser study suggests that bubbles in ground water contained in fissures or pockets surrounding hot magma could be the source of tremor[20], and quantitative studies of this mechanism are now in progress[34]. Because we know neither the dimensions of the conduits containing the fluid nor the nature of the fluid that is causing the seismicity at volcanoes, this is a very difficult problem. The study of Old Faithful, where at least constraints can be put on the fluid and on the conduit dimensions, has been important in developing the volcanic ideas. Fluids proposed for the source of volcanic tremor (undersaturated magma, gassy magma, water) can have sound speeds that differ by nearly three orders of magnitude, and the above discussion suggests that there will be an ambiguity in decoupling the effects of conduit dimensions from fluid properties in any analysis of volcanic harmonic tremor. This is an active area of research in volcanology because of the regular occurrence of volcanic tremor at some volcanoes near heavily populated areas where forecasting has enormous implications for life and economy; e.g., at Ruiz Volcano in Columbia. Fluid dynamicists can potentially contribute important ideas and measurements to this problem: laboratory studies of the dynamics of large collapsing bubbles and of two-phase flow in long pipes of variable area are needed. In particular, theoretical and experimental work on the dynamics of compressible flow with gravitational effects will be required to deal with problems involving these fluids at geologic scales.

V. Mount St. Helens: a supersonic jet

A. Geologic setting

Mount St. Helens became famous as an "active volcano" on May 18, 1980. However, that eruption was heralded by nearly six weeks of precursor activity during which eruptions were strikingly similar in scale, frequency, and fluid dynamics to eruptions of major geysers like Old Faithful. On March 27, 1980, after a repose of one century and ominous seismicity for a week, an unobserved eruption created a small crater in the summit of the mountain. For a few weeks, eruptions of steam and ash emanated from the summit (Fig. 27). Studies of deformation of the mountain, and later events, strongly suggest that magma was being intruded into the edifice from depth at this time (Fig. 28a). Water near the magma was heated and convected upward, emerging in eruptions that were geyser-like in scale (hundreds of meters to a few kilometers high), duration (minutes to tens of minutes), and frequency (every few hours). These early eruptions were driven by heated ground water -- no magma was involved.

FIG. 27. A geyser-like eruption of Mount St. Helens, April 1, 1980. An ash-laden density flow rolls down the southwestern slopes (to the right in the photo) from the summit crater at about 2,930 m (9,670 ft) elevation, while steam separates and rises to about 4,500 m (15,000 ft). The fluids in the density current and in the dusty steam might be quite well modeled by pseudogas approximations, because they are relatively dilute. Photo by H. and S. Kieffer.

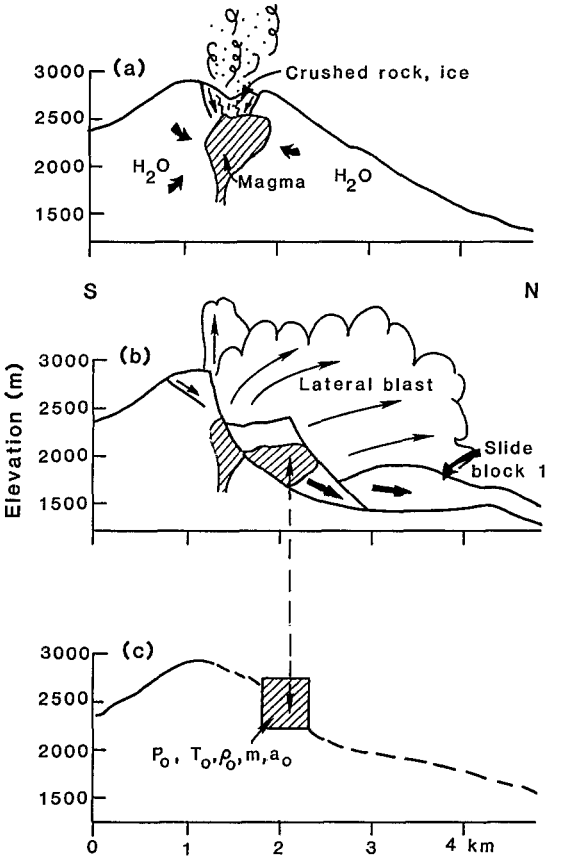

FIG. 28. (a) South-to-north cross section showing schematically the conditions inside Mount St. Helens during March, April, and early May, 1980. Magma has moved high into the mountain. Water heated by the magma has risen through fractures and erupted (a typical eruption is shown in Fig. 27), creating a conduit and summit crater. Crushed rock, ice, ash, and water that intermittently choked the conduit were reworked by successive eruptions. (b) Reconstruction[36] of the initiation of the lateral blast on May 18. The mountain failed along three major faults (indicated by arrows). Magma was present in each, but appeared to emanate mainly from slide block 2 (shown in motion) and slide block 3 (indicated on top of the south part of the mountain). (c) Schematic drawing of initial conditions assumed for the fluid flow model. The complex structure of the landslides has been simplified, and the reservoir is approximated as a single volume whose dimensions are given in the text. In spite of the complicated time history of the landslides, the triggering is assumed to be instantaneous for modeling purposes. The material erupted was partially magmatic and partially hydrothermal. Only the top part of the source shown in (a) and (b) would have been erupted into the lateral blast. The remainder was erupted into a tall vertical eruption column during the several days after the lateral blast. The magma properties are assumed homogeneous at initial pressure, P_0, temperature, T_0, density, ρ_0, and sound speed, a_0 (calculated for a pseudogas with mass loading m).

Although these eruptions were more geyser-like than "volcanic," they differed thermodynamically from eruptions of most geysers because the erupting vapor carried a heavy load of particulate material -- crushed rock and ice gouged from the conduit and crater (this particulate material gives the lower part of the eruption plume in Fig. 27 a dark color). The mass loading by this material affected the thermodynamics in two ways: the entrainment of solid fragments increased the bulk density of the fluid, and heat transfer between the solids and the expanding gas altered the expansion of the gas from that which would be obtained by a two-phase mixture or vapor alone. In the pseudogas approximation discussed in Section II, mass loading is taken into account as an increased molecular weight of the mixture (see the equations at the top of Fig. 4). Heat transfer from hot particles to cooler vapor is accounted for by a decrease in the isentropic exponent of the perfect-gas law. The expansion of a mass-loaded vapor is contrasted with the expansion of a vapor alone, or a decompressing liquid, in Fig. 29. As can be seen from this figure, under some circumstances mass loading can simplify the fluid dynamics by preventing phase changes -- the entropy of a gas phase is increased by heat conducted from solids, and thus formation of a condensed phase is suppressed. However, complications of heat transfer, drag, and interparticle interactions arise. No theoretical models yet handle these effects realistically for the range of particle sizes, particle shapes, and mass loading typical of volcanic eruptions.

The north flank of Mount St. Helens was badly fractured and weakened by the intrusion of magma in March and April, 1980. At 8:32 a.m. on May 18, a magnitude 5.2 earthquake shook the mountain, and several large landslide blocks broke loose and slid downhill toward the North Fork of the Toutle River (Fig. 28b). Within a few seconds, the pressure on magma, hot water, and gases inside the mountain was greatly reduced, and their rapid expansion produced the devastating event that was to become known as the "lateral blast". The evolution of this blast was recorded by several eyewitnesses, by seismic equipment stationed around the mountain, by weather barometers, and by damage to the environment and to man-made equipment around the mountain[35]. Nearly 600 km^2 of forest were devastated, and approximately 60 people were killed. Heavy logging equipment was tossed and overturned (Fig. 30a); trees were totally stripped from the land over a large area. Where they remained, as much as 10 cm of bark and wood was abraded and the interiors were impregnated with shrapnel (Fig. 30b). The pattern of tree blowdown (Fig. 31) provided a remarkable record of local flow directions -- certainly a flow-field pattern to challenge geologists and fluid dynamicists for years to come.

In the region closest to the volcano, trees were either stripped from the land or were felled subradially away from the vent, and the blowdown direction showed little dependence on the terrain (Fig. 32). This zone is called the *direct blast zone*, to emphasize that the blast travelled directly away from the mountain without regard to even major topographic obstacles[37]. Surrounding the direct blast zone is a zone in which topography did influence the blowdown direction, called the *channelized blast*

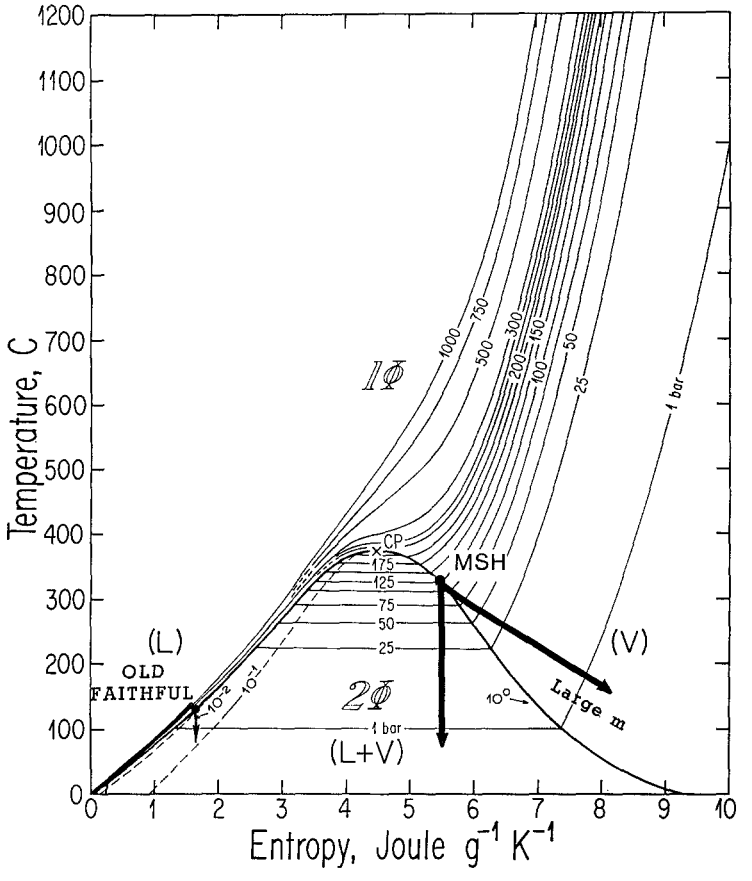

FIG. 29. Temperature-entropy diagram for H_2O with isobars. On the left, an isentrope for an eruption of Old Faithful is shown; on the right, two isentropes for eruptions from the assumed Mount St. Helens (MSH) initial conditions are shown. Pure steam would have condensed during isentropic expansion, as indicated by the vertical line. Heavy mass loading of the steam by hot particles increases the mixture entropy and, by transfer of heat to the steam, increases the entropy of the steam during expansion. Condensation during decompression is thereby prevented, as indicated by the arrow pointing to the lower right.

zone to emphasize that the blast followed channels in the topography. Surrounding this region and marking the limits of the devastated area is the *singed zone*, a zone in which trees were left standing but were singed by the heat of the blast as it became positively buoyant and lifted from the ground into the atmosphere[37].

This devastation was caused by the eruption of more than 10^{14} g of magma, hot water, and entrained glacier ice and trees. The vent through which the material emerged covered a large fraction of the north side of the mountain. Available evidence allows

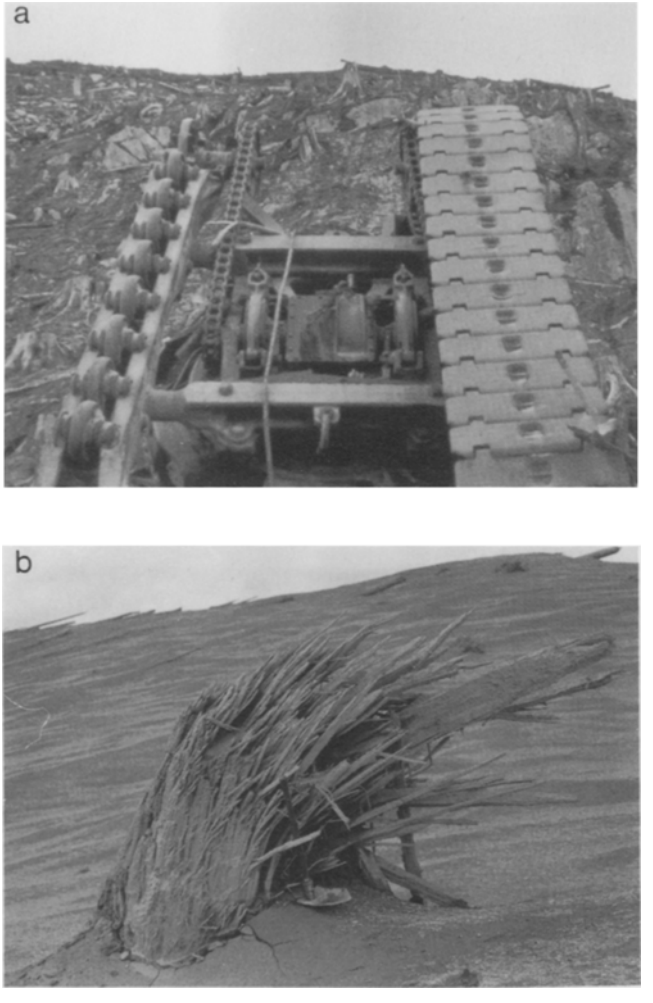

FIG. 30. Photographs showing (a) damage to heavy logging equipment during the May 18 lateral blast, and (b) damage to trees. Photos by H. and S. Kieffer.

many theories, and geologists do not even agree on initial and boundary conditions for the flow[38]. I describe below my model for the blast, a model that emphasizes the role of gas expansion and nozzle flow[37]. Given a plausible set of simplifying assumptions, this model attempts to define the flow characteristics and to correlate these predicted characteristics with features in the devastated area: tree directions; the transition from direct to channelized blast zones; measured velocities and temperatures; and the general shape of the devastated area.

B. A simple nozzle model

In my model, the lateral blast is simplified to the problem of the eruption of a pseudogas from a reservoir under pressure into an atmosphere at lower pressure. The

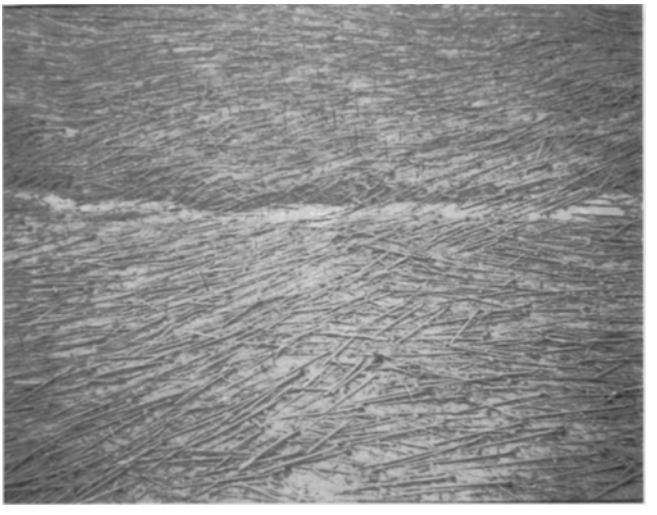

FIG. 31. Typical pattern of tree blowdown. Note that the tops of the trees and most of the small limbs are missing. The contrast in this photo is low because volcanic ash mantled trees and slope when the photo was taken shortly after May 18, 1980.

thermodynamic properties and reservoir geometry are also simplified accordingly (Fig. 28c). The fluid is defined by its initial (average) pressure, P_0; temperature, T_0; and mass ratio, m, of solid to vapor phases. The reservoir is assumed to have resembled a converging nozzle whose exit plane (vent) was the landslide scarp left on the north face of the mountain by the removal of the avalanche material.

Although the model can easily be scaled both geometrically and thermodynamically, one set of plausible values for initial conditions demonstrates the features of the model: an average reservoir pressure of 12.5 Mpa (125 bars, the pressure appropriate to 650 m of rock overlying the reservoir), an initial temperature of 600 K (327 °C), and a mass ratio of rock to steam of 25 : 1. The initial temperature assumed may seem surprisingly cool if one only associates volcanic eruptions with red-hot, incandescent magma. However, many so-called "volcanic" eruptions, such as the one shown in Fig. 27, are not driven by magma, but by heated water ("phreatic eruptions"), or by a mixture of heated ground water and magma ("phreatomagmatic eruptions"). The detailed nature of the volcanic gases driving the eruption is ignored here because the large-scale features of the fluid mechanics are probably not sensitive to the gas source. The chosen temperature happens to be the saturation temperature of pure water at 12.5 Mpa (125 bars), and it is a reasonable number to assume *a priori* if one believes that geothermal waters heated to saturation conditions drove the eruption (and that the badly fractured mountain edifice could not sustain any overpressure in the eruptive fluid). The temperature of 600 K can also be thought of as an average temperature for a complex mixture which, after it had traveled only a short distance, contained material ranging

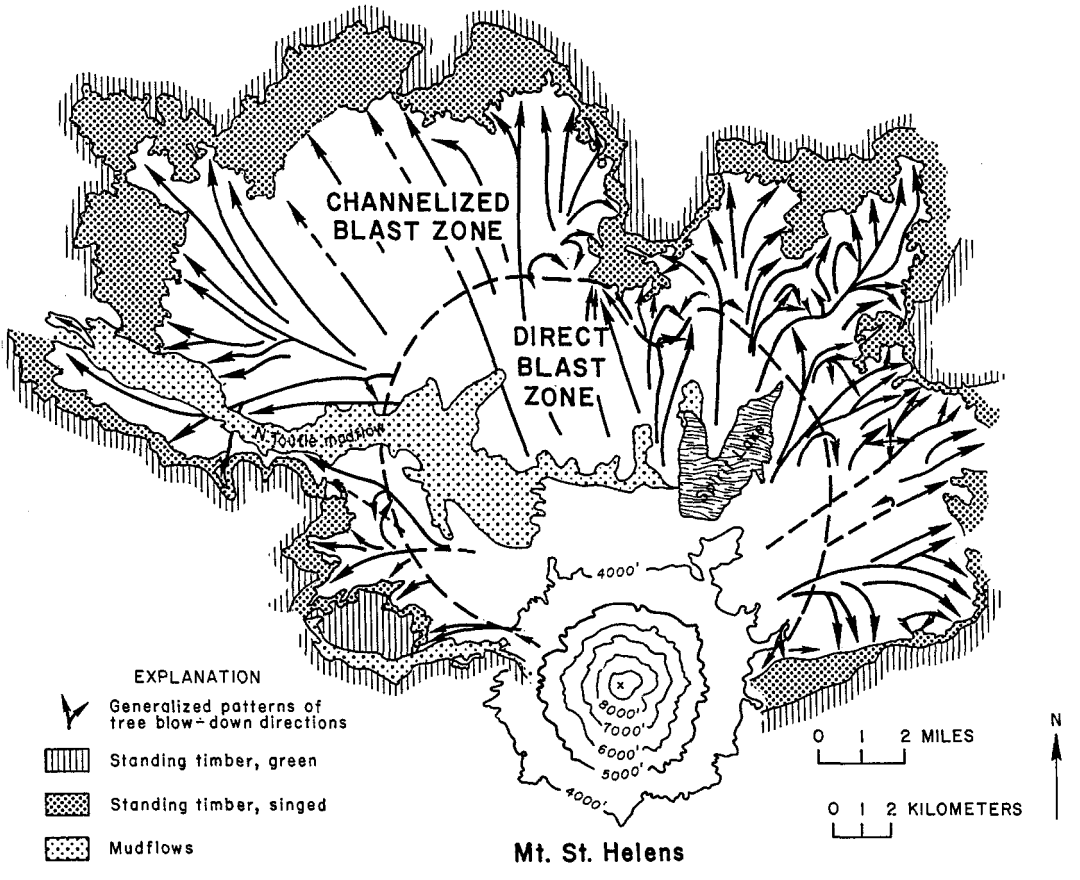

FIG. 32. Map showing generalized direction of tree blowdown, with approximate extent of direct, channelized, and singed zones.

from the melting temperature of the magma (~ 950 °C) to the freezing temperature of glacial ice and snow entrained in the flow. Reasonable changes in assumed initial pressure, temperature, and solid-to-mass ratio do not qualitatively alter the conclusions. Atmospheric pressure is taken as 0.87 bar. For scale, the vent diameter is taken as 1 km, the approximate width of the scar left by the avalanches. The eruption is assumed to be centered at 2,135 m (7,000 ft), and the centerline of the flow is oriented about 5 degrees east of north to match the overall direction of the flow field. These are the only variables in the model -- there are no arbitrary fitting parameters.

Nozzles operating at pressure ratios much greater than about 2:1 are supersonic. At the ratio of 125 : 0.87 assumed above for Mount St. Helens, the emerging flow should have been highly supersonic (refer to Fig. 2; see Fig. 33 for a more detailed diagram and nomenclature). The most important dynamic parameter of the erupting fluid is its sound speed -- 105 m/s for the reservoir fluid postulated above, according to pseudogas calculations. This sound speed is about 1/3 of the value of the atmospheric sound

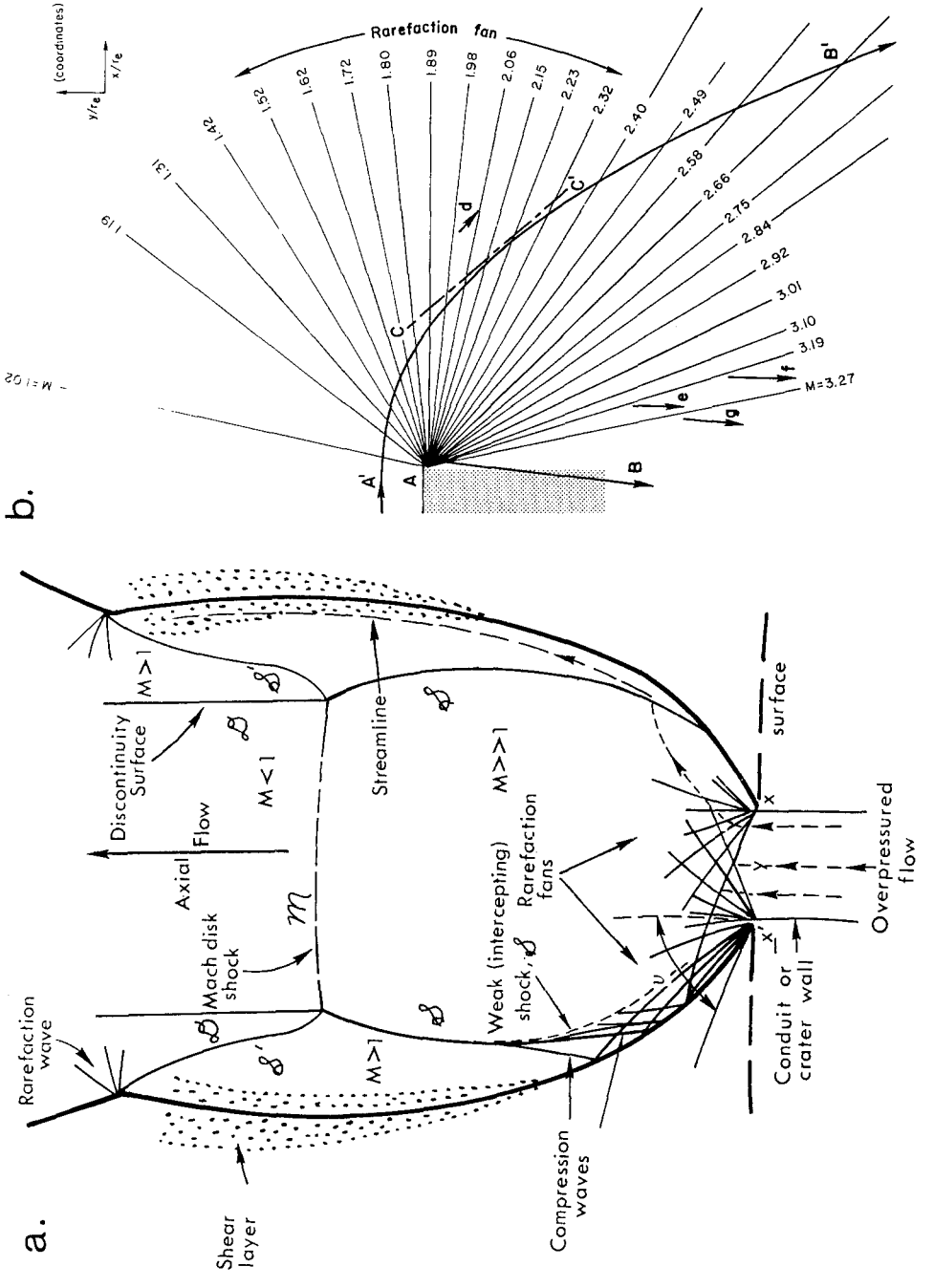

FIG. 33. (a) Schematic diagram of the structure of an underexpanded supersonic jet[39]. The flow leaves the nozzle through plane xx′. Further discussion of this figure is given in Ref. 37, p. 388. (b) Detail of a corner rarefaction for conditions appropriate to the Mount St. Helens model. This could be interpreted as a map view of the flow pattern

from the east corner of the vent (where the walls of the volcano are projected by the stippled pattern). The (mathematical) characteristics of the flow are the thin lines that radiate from the corner A of the vent. They are labeled according to the Mach number, M, of the flow as it crosses the characteristics. AB and A′B′ are streamlines of the flow; CC′ is a tangent to A′B′. The small arrows d, e, f, and g represent calculated local directions of flow as they would be recorded in the directions of tree blowdown. The arrows e, f, and g are particularly significant, because if these are assumed to lie along flow streamlines and are extrapolated linearly backwards, a flow source significantly in front of the mountain would be inferred. In compressible flow, linear extrapolation of streamlines cannot be made, because the curvature of the flow through expansion waves would not be properly accounted for.

speed. Therefore, the flow field of the volcanic pseudogas can be *internally supersonic*, but still *subsonic* with respect to the surrounding atmosphere. Thus, there is no contradiction between the postulated supersonic flow and the notable absence of atmospheric shock waves during the lateral blast (see eyewitness accounts in Ref. 35 and Ref. 37).

Consider first the initial velocity of the fluid. According to the proposed model, the fluid would accelerate from rest in the reservoir to sonic velocity at the vent -- 100 m/s. Laboratory studies[40] have shown that, in the absence of gravitational effects, the flow-front velocity of dense fluids remains at approximately the sonic velocity for many source diameters, because entrainment of the light surrounding atmosphere causes very little deceleration. At Mount St. Helens, the flow would have accelerated as it dropped down the face of the mountain into the valley of the North Toutle River, but it would have decelerated as it rose back up into the high country north of the Toutle River (the region now called Johnston Ridge). Because the combined effects of gravity and compressibility are not included in the model, it cannot be accurate to this level of detail. Measured velocities of the flow, averaged over substantial topographic relief to Johnston Ridge, were about 100 m/s, in good agreement with the calculated sonic velocity.

According to the model, the fluid emerged from the volcano as an under-expanded supersonic jet (Fig. 34). The pressure would have decreased to 7.5 Mpa (75 bars) as the fluid accelerated from the reservoir to the vent, and then decreased to ambient pressure through a series of complex rarefaction waves and shock waves within the jet outside of the volcano, as shown schematically in Fig. 33a and in detail in Fig. 34. Because of the high pressure in the jet as it left the vent, it would have spread laterally through a characteristic angle known as the *Prandtl-Meyer angle* (Fig. 33b). For the initial conditions postulated, the Prandtl-Meyer angle is 96 degrees. Thus, flow that initially was directed northward by the geometry of the vent would have diverged to the east and west; note this type of expansion beyond the east-west line in Fig. 32. The predicted

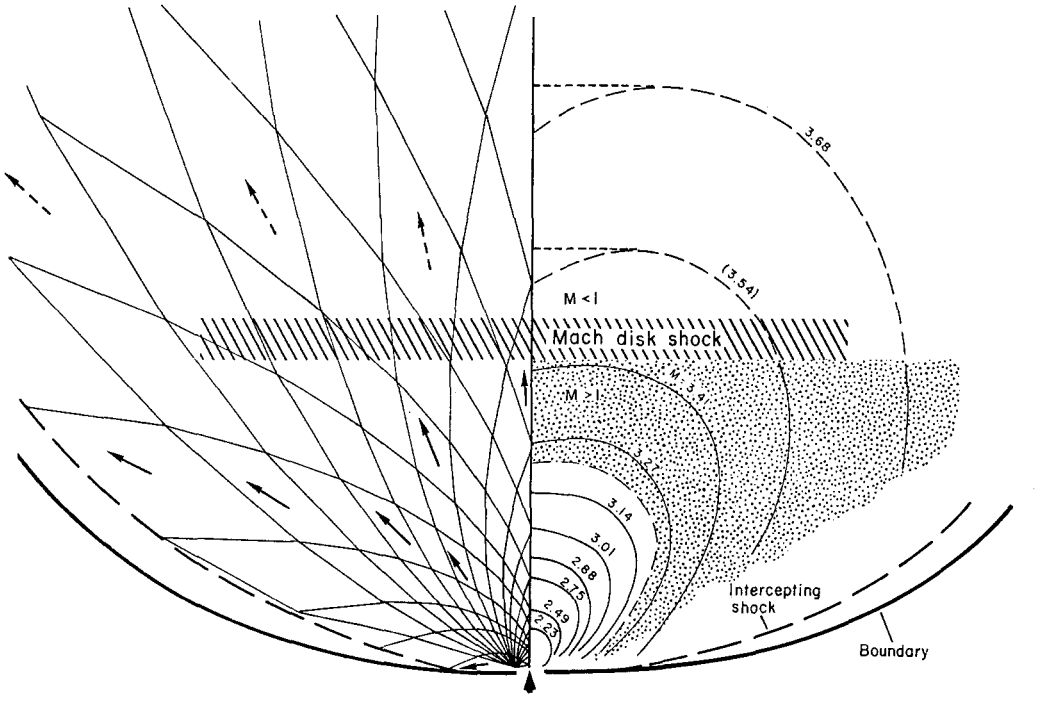

FIG. 34. Map of the flow field according to the present model of blast dynamics[37]. To ease the numerical computations, the exit Mach number of the flow is assumed to have been 1.02, instead of the sonic Mach number 1.00. All length dimensions are normalized by the vent diameter. The model is symmetric about the axis of the vent and is split into two halves here for conciseness. On the left, the characteristics (computed by hand) are shown as thin lines radiating from the corner of the vent. The boundary of the flow is assumed to have been at constant pressure (0.87 bar). The peripheral intercepting shock formed by reflection of the expansion waves from this boundary is shown as a dashed line. Note how reflection of expansion waves deflects the boundary of the flow away from its original expansion angle of 96 degrees. Flow directions are shown by representative arrows, solid within the zone where the model is strictly valid, dashed in the zone where the model is extrapolated across shock waves. On the right, contours of constant Mach number M and, therefore, constant pressure (P/P_0), temperature (T/T_0), and density (ρ/ρ_0) are shown. Velocities are given implicitly by the Mach numbers. Each contour is labeled by the value of the Mach number, M. From the innermost contour outward, values of M, P/P_0, T/T_0, and ρ/ρ_0 are given. In the supersonic region, these values are, respectively, (2.23, 0.087, 0.91, 0.095); (2.49, 0.047, 0.89, 0.053); (2.75, 0.025, 0.87, 0.029); (2.88, 0.018, 0.86, 0.021); (3.01, 0.013, 0.85, 0.016); (3.14, 0.009, 0.83, 0.011). The values extrapolated into the subsonic zone were used by the author in Ref. 37 to extrapolate the flow density to the singed zone, but should be ignored, because a more realistic assumption is that the flow returns to atmospheric pressure. The area covered by a stippled pattern is a core in the

flow that is at subatmospheric pressure. Downward curvature of the outer contours near the axis of the flow is probably an artifact of the grid size used in the numerical solution, and the likely contour shape is shown by short dashed lines. A computer model that produced a somewhat smaller supersonic zone, because the flow boundary was assumed to be inviscid rather than viscous (as in the above model), was run by R.A. O'Leary, Rocketdyne, for the author. Details can be found in Ref. 41. Differences between the two models are not significant in terms of our lack of knowledge of the real complexities of the eruption; e.g., material emerging from two moving landslides instead of from a single vertical vent.

flow zone is superimposed on the map of the devastated area in Fig. 35. I suggest that the devastated area has a southern boundary that actually curves south of an east-west line near the volcano because the initial Prandtl-Meyer expansion drove gas around in these directions.

In an under-expanded supersonic jet, rarefactions crisscross the flow and reflect off the flow boundary, assumed to be at a constant pressure equal to ambient atmospheric pressure (Fig. 33a). Upon reflection, they turn into weak compressive shocks called "intercepting" or "barrel" shocks (Fig. 33a). The reflection of the rarefactions from the flow boundary turns the diverging flow back toward a more axial direction. I suggest that these reflections are responsible for focusing the direct blast zone so strongly to the north (Figs. 32 and 35) and for limiting the extent of east-west devastation.

The fluid inside of the jet expands and accelerates as it passes through the expansion waves -- obtaining, according to the model, a Mach number of more than 3 on the centerline and velocities in excess of 300 m/s. Internal velocities can be locally higher than the flow-front velocity because of the internal rarefaction and shock waves. Pressure, temperature, and density decrease through the expansions. The pressure behavior is particularly interesting and illustrates the nonlinearity of the supersonic expansion process: as the fluid expands, the pressure decreases *below* atmospheric pressure, and a large zone of subatmospheric pressure develops inside the supersonic zone (see the shaded area in Figs. 34 and 35). The existence of such a low-pressure core has some interesting volcanologic implications; for example, plastic components on vehicles in or near this part of the devastated area were degraded by the formation of large vapor bubbles[42]. Laboratory studies demonstrated that the vapor formation was caused by exposure of the plastic to high temperatures during the blast. Efforts to duplicate the degradation by heating similar plastics in the laboratory under atmospheric pressure produced general similarities, but failed to reproduce the large size of the bubbles found on the components from the vehicles. I speculate that bubbles may have grown unexpectedly large because the external pressure was temporarily lower than atmospheric in the supersonic core of the lateral blast.

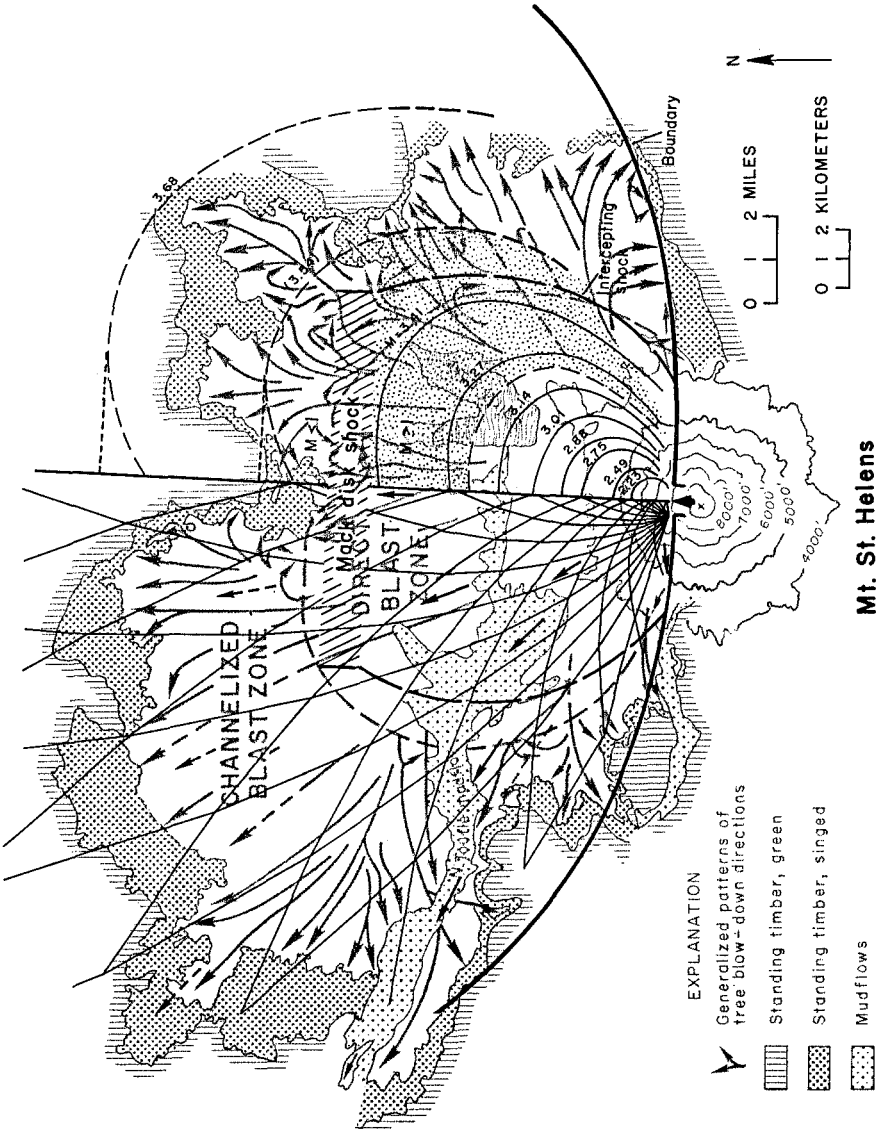

FIG. 35. The model of Fig. 34 superimposed on the map of the devastated area. The coincidence of the Mach disk with the direct blast zone boundary in the northerly direction suggested to the author that the direct blast zone was a zone of strong supersonic flow.

In an under-expanded jet, the intercepting shocks strengthen within the flow and coalesce across it into a strong shock standing perpendicular to the axis of the flow. This shock is called the *Mach disk* (Fig. 33a). As gas flows through the shock, it decelerates from supersonic to subsonic conditions; to a first approximation, the pressure on the downstream side of the Mach disk is atmospheric. Inertia of the heavy

debris entrained by the blast at the Mach disk (the overturned logging vehicle in Fig. 30a and the debris around it give some impression about the size of the debris load near the Mach disk), would propel the particulate matter through a "gas shock", so that the Mach disk should, in this geologic case, be thought of as a Mach-disk zone, perhaps of the order of 1 km in thickness. As the fluid decelerates into the subsonic zone downstream of the Mach disk, flow velocities decrease, pressure rises from subatmospheric back toward atmospheric, and the density of the fluid increases. According to the calculations, the Mach disk would have stood about 11 km north of the vent. The calculated position and, to a lesser extent, the position of the lateral intercepting shocks, coincide roughly with the boundaries between the direct and channelized blast zones (Fig. 35). I propose that these two zones correspond roughly to the boundary between supersonic and subsonic flow regimes within the lateral blast.

Because of the dramatic deceleration of the flow at the Mach disk, gravity, which was not a dominant force within the direct blast zone, dominated flow mechanics outside of this zone -- in the channelized blast zone. Thus the flow streamlines, as indicated by the tree blow-down patterns, are more influenced by topography in the channelized, subsonic zone. The devastated area therefore consists of two parts: the inner direct blast zone in which gas dynamics effects and supersonic flow were probably dominant, and the surrounding channelized blast zone in which downhill flow driven by gravity was probably dominant. This is an oversimplification, because both effects were probably important throughout much of the devastated area (e.g., the most highly supersonic zone and the Mach disk happen to coincide with a region of very steep topography), and quantitative modeling including both effects is required in the future.

Temperatures throughout a particle-laden flow like the lateral blast are remarkably high and uniform because of the high mass ratio of solids to vapor (this is the effect of $\gamma \sim 1$; see Fig. 4 and Eq. 2). Calculated temperatures changed only from 600 K to 480 K at limits of the devastated area; these temperatures are in excellent agreement with temperatures measured in the deposits immediately after the eruption[35].

Several other properties of the blast can be calculated from this model. For example, the maximum mass flux is calculated to have been 10^4 g/s/cm^2, and the thermal flux to have been 2.5 MW/cm^2. The total energy of the blast was 24 Mt, of which 7 Mt was dissipated during the blast itself, and the remaining 17 Mt was dissipated during the almost simultaneous condensation of steam in the blast and the subsequent cooling of steam and rock to ambient temperature in the weeks following May 18.

As mentioned above, the supersonic flow model for the lateral blast has been controversial. Nevertheless, features analogous to those eroded into the surfaces of supersonic reentry vehicles have been found in the erosion surface under the blast deposits[43].

C. Comparison of Mount St. Helens with the Saturn V rocket

The magnitude of the blast can be impressed upon one's imagination, and the true scale of nozzles in geology can be appreciated, by comparing the Mount St. Helens blast with a Saturn V F-1 liquid-oxygen/kerosene motor (Fig. 36). The mass flux per unit area at the exit of an F-1 is about 25 g/s/cm^2; that of the lateral blast was 240 times as great. The power per unit area of the F-1 motor is approximately 0.8 MW/cm^2; that of the lateral blast was three times greater. The Saturn V power is delivered over five rockets covering roughly 50 m^2; the power at Mount St. Helens flowed out of a vent more than 2,000 times this area. The total power of the five Saturn V motors is about 4

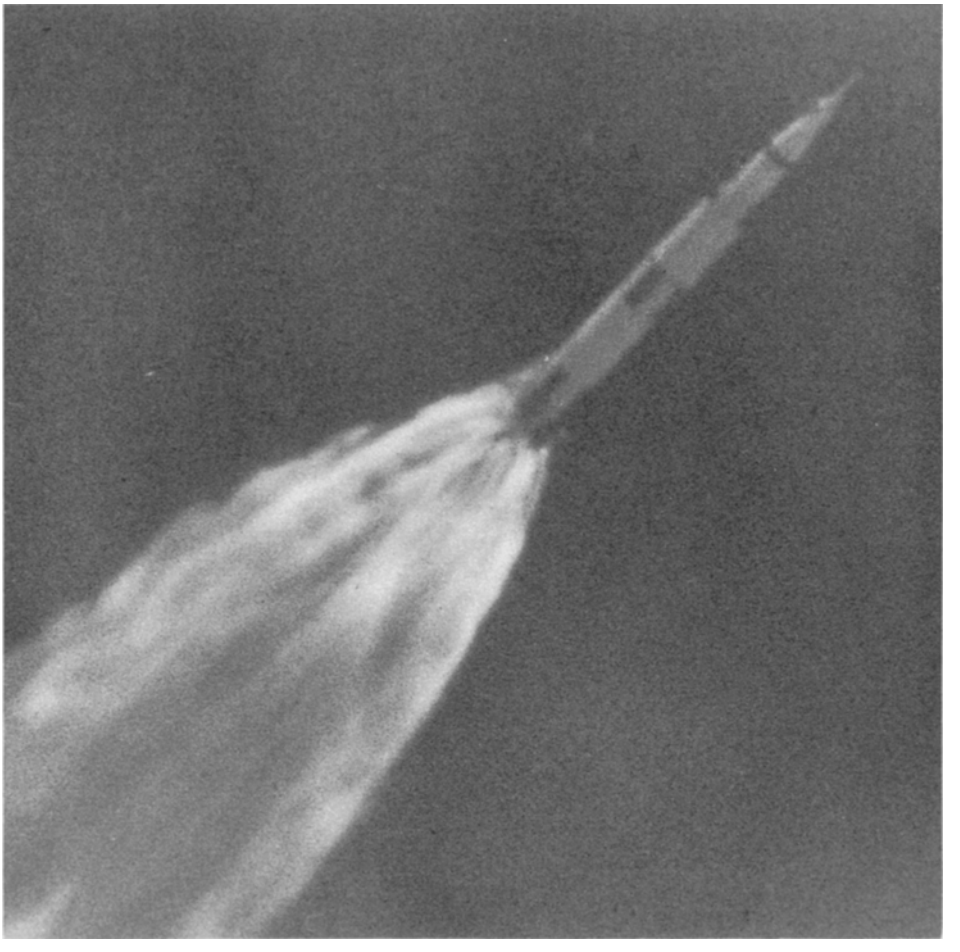

FIG. 36. A comparison of the power of Mount St. Helens with that of a Saturn V F-1 rocket engine is given in the text. Five F-1's provided the power needed to launch the Apollo spacecraft. The photograph shows Apollo 10 shortly after launch from the Kennedy Space Center on 18 May, 1969 (courtesy of NASA).

$\times 10^5$ MW; that of the blast was nearly 16,000 times greater. The thrust of the Saturn V is 7.5 million pounds (3.3×10^7 N); that of the blast was nearly 10^5 greater. The lateral blast of May 18, 1980, was indeed an awesome event by both geologic and fluid dynamical standards.

VI. Perspectives

In the discussion of Crystal Rapids and Old Faithful Geyser, I have pointed out specific directions for future research. At Mount St. Helens, unequivocal re-creation of the fluid dynamics of the lateral blast may be difficult in spite of the fact that it is the best-documented violent volcanic eruption in recorded history. The observational problems inherent in geologic research, and particularly in the monitoring of geologically rare events, are enormous. Nevertheless, the evolution of fluid dynamics in geology over the past few decades has been rapid; viz., the pioneering work of Wilson and Sparks and their colleagues and students[44].

It is appropriate to conclude with the thought that the development of modern spacecraft, in which Hans Liepmann and his colleagues have been so involved, has led to one of the most exciting discoveries of modern times -- the existence of erupting volcanoes on another planet[45]. Even as we struggle to document and understand the geological physics of fluids in our world, we have already discovered new puzzles in fluid dynamics on other worlds.

Acknowledgements

The studies described here have extended over 12 years and have involved many colleagues to whom I owe thanks, including those I have referenced or mentioned as "private communication" in this article, and numerous others who could not be referenced because of space limitations: colleagues who work within the National Science Foundation, the U.S. Geological Survey, and the Bureau of Reclamation to help fund the work; and Eugene Shoemaker and Bradford Sturtevant, who interested me in, and taught me, fluid dynamics as a student from the text by Liepmann and Roshko. Finally, special thanks are owed to a supportive husband who has encouraged all my work, and to our son -- who proved a valuable field assistant as early as 1976 at the age of 10 (on many Yellowstone field trips by providing hot dogs and comics to mom, who was waiting yet another few hours for a geyser to erupt), and in 1987 could still be found enjoying helping mom carry equipment in and out of the Grand Canyon.

References and footnotes

1. Approved for publication by Director, U.S. Geological Survey, January 23, 1986.
2. For example, see H.W. Liepmann and A. Roshko, *Elements of Gasdynamics* (Wiley, New York, 1957). For the sake of brevity, references in this paper are

limited. The author has published detailed analyses of the three geologic problems discussed here in the references cited below, and the reader will find references to other relevant work in those papers.

3. This analogy was apparently first described by D. Riabouchinsky, C. R. Acad. Sci. **195**, 998-999 (1932). For a more accessible reference, see *Modern Developments in Gas Dynamics*, edited by W.H.T. Loh (Plenum, New York, 1969), pp. 1-60.

4. For example, see P.A. Thompson, *Compressible-fluid Dynamics* (McGraw-Hill, New York, 1972), pp. 517-531.

5. In the spirit of emphasizing the similarity of the various flow fields discussed in this paper, the word "nozzle" will be used interchangeably with the words "flume", "channel", and "conduit", and the word "contouring" will be used interchangeably with the word "eroding".

6. "Low" pressure ratio in this context means that the reservoir pressure is less than about 2 times atmospheric pressure; see, for example, the tables of isentropic flow variables given in M.J. Zucrow and J.D. Hoffman, *Gas Dynamics* (Wiley, New York, 1976).

7. Although schematic illustrations of the structure of supersonic gas jets can be found in most textbooks on gas dynamics, collections of actual photographs are rare. One such collection is E.S. Love and C.E. Grigsby, NACA RM L54L31 (1955).

8. A "small" head difference means that the elevation difference between the two reservoirs should not exceed approximately one-third of the head of the source reservoir.

9. Collections of illustrations of subcritical flow accelerating to supercritical flow in a converging-diverging channel are rare. Some examples can be found in E. Preiswerk, NACA TM 935 (1940). Illustrations of supercritical flow in converging and diverging channels can be found in the four papers in High-velocity Flow in Open Channels: A Symposium, Paper 2434, Trans. ASCE **116**, 265-400 (1951).

10. Reviewed in S.W. Kieffer, J. Geophys. Res. **82**, 2895-2904 (1977).

11. S.W. Kieffer and J. Delany, J. Geophys. Res. **84**, 1611-1620 (1979).

12. K. Richards, *Rivers: Form and Process in Alluvial Channels* (Methuen, London, 1983), p. 58.

13. As an example of the relative magnitudes of Froude and Mach numbers, consider order of magnitude estimates for Old Faithful and for the Mount St. Helens lateral blast. At Old Faithful, the exit velocity is ~ 80 m/s (see text, Section IV D). As

the hottest fluid (116–118 °C) ascends through the conduit to the exit plane, it becomes a two-phase mixture with about 4 weight percent vapor, for which the equilibrium sound speed is about 57 m/s at 0.8 bar atmospheric pressure at the elevation of Old Faithful. This gives a Mach number of ~1.5, indicating that compressibility effects are important. An internal (densimetric) Froude number for the jet of Old Faithful can be calculated (see Section IV D). For Old Faithful, I take nominal values of jet velocity = u = 80 m/s, jet density = ρ_0 = 11.2 kg/m^3 (decompression of 116 °C water isentropically to 0.8 bar, 93 °C, 4 percent vapor), atmospheric density = ρ_a = 0.7 kg/m^3, and an equivalent axially symmetric conduit diameter = D = 1.1 m. With these parameters, the square root of the densimetric Froude number (which is the value to be compared with a Mach number) is 25. The jet is negatively buoyant because $\rho_0 > \rho_a$. An internal Froude number for the Mount St. Helens lateral blast, considered as an incompressible density flow on an inclined plane, can be calculated from $Fr = u/(g'd \cos\theta)^{1/2}$, where $g' = g(\rho_a - \rho_0)/\rho_0$ (the absolute value of this quantity is taken); ρ_0 is the density of the jet; ρ_a is the density of the atmosphere, assumed uniform; d is the flow thickness; and θ is the slope angle. For nominal parameters, I take a flow density of 100 kg/m^3 (g' = 9.7 m/s^2), θ = 11 degrees, u = 100 m/s, d = 100 m. For these parameters, Fr ~ 3.2. This represents a minimum estimate, because internal flow velocities may have been greater by a factor of two to three. Note that the observed velocity of the front of the blast (100 m/s) is nearly identical to the sound speed of a pseudogas laden with solid fragments at a mass ratio of 25/1 (see Ref. 37), so that M ~ 1. These order-of-magnitude estimates demonstrate that quantitative models for the flow fields of Old Faithful and the Mount St. Helens lateral blast must eventually consider both compressibility and gravity effects.

14. The values of constriction used to obtain Fig. 6 were inferred by measuring the width of the surface water in the photo series of the 1973 U.S. Geological Survey Water Resources Division, one of which is shown in Fig. 5. From measurements of surface width, the constriction at Crystal Rapids in Fig. 5 is 0.33, and it plots as the left-most block in Fig. 6. However, for purposes of hydraulic modeling later in the discussion, it is necessary to assume an idealized cross section for the channel. A rectangular cross section is assumed. In this simplification, the "average" constriction used for modeling is generally less than that measured from air photos, because the shallow, slow flow across the debris fan, which shows in air photos of the water surface but accounts for only a small fraction of the total discharge, is ignored. In the case of Crystal Rapids, the model value is 0.25, so the reader should be alerted to this change in "shape parameter" when the modeling calculations are discussed. By either criterion used to determine the shape parameter, the channel at Crystal Rapids was more tightly constricted than at the older debris fans that formed before Glen Canyon Dam was emplaced.

15. Because of the common usage of cfs in hydraulics and by river observers, volume flow rates are given in both metric and English units throughout this paper.

16. Details given in S.W. Kieffer, J. Geol. **93**, 385-406 (1985).

17. The backwater above Crystal Rapids extends as much as 3 km upstream and is affectionately dubbed "Lake Crystal" by river runners.

18. The past tense is used in this discussion because the events of 1983 modified Crystal Rapids, and these calculations are not appropriate to its current configuration.

19. The calculations described here attribute all changes in flow regime to lateral constriction, because of the assumption of constant specific energy. In all rapids there are changes in bed elevation that affect the total and specific energy of the flow and, therefore, affect the transition from subcritical to supercritical conditions. The words "subcritical" and "supercritical" as used in this section therefore apply to a large-scale condition of the rapid, not to local details, because these additional effects are not accounted for. Most rapids are weakly supercritical because of changes in bed elevation, even in the regime called "subcritical" in this section. There are also substantial small-scale irregularities in bed topography, such as ledges and rocks, that cause local supercritical flow. The behavior of the river in flowing around such obstacles is not included in this generalized discussion.

20. S.W. Kieffer, J. Volc. Geoth. Res. **22**, 59-95 (1984).

21. C.O. McKee, D.A. Wallace, R.A. Almond, and B. Talais, Geol. Survey, Papua New Guinea Mem. 10, 63-84 (1981).

22. F. Birch and G. Kennedy, in *Flow and Fracture of Rocks*, Geophys. Monogr. Ser. **16**, 329-336 (1972).

23. Summarized in S.W. Kieffer and J. Westphal, EOS: Trans. Amer. Geophys. Union **66** (46), 1152 (1985); details in preparation.

24. D.E. White, Amer. J. Sci. **265**, 641-684 (1967).

25. S. Fujikawa and T. Akamatsu, Bull. Japan Soc. Min. Eng. **21**, 223-230 and 279-281 (1978).

26. For example, see L. Biasi, A. Prosperetti, and A. Tozzi, Chem. Eng. Sci. **72**, 815-822 (1972).

27. W. Hentschel, master's thesis (Göttingen, 1979); also Fortsch. Akustik, DAGA'80, Berlin, p. 415-418.

28. The geometry of the conduit determines whether the conduit should be considered open-ended or closed-ended. Since no probe has demonstrated a large reservoir at the bottom of the conduit, it is treated here as a closed pipe. Resonant frequencies of an open pipe would be half of those calculated from this formula.

29. J.S. Turner, J. Fluid Mech. **26**, 779-792, 1966; C.J. Chen and W. Rodi, *Vertical Turbulent Buoyant Jets -- A Review of Experimental Data* (Pergamon Press, New York, 1980).

30. G.B. Wallis, *One-Dimensional, Two-Phase Flow* (McGraw-Hill, New York, 1969), and references cited therein.

31. F.J. Moody, Trans. ASME J. Heat Transfer **87**, 134-142, 1965, as reviewed by Wallis (Ref. 30, p. 48).

32. H.K. Fauske, ANL Report 6633, 1962, as reviewed by Wallis[30].

33. S. Fuller and J. Schmidt, *Yellowstone in Three Seasons* (Snow Country Publications, Yellowstone National Park, Wyoming, 1984).

34. R.C. Leet, J. Geophys. Res., in press; contains review of other models for volcanic tremor.

35. Many detailed articles about Mount St. Helens can be found in P.W. Lipman and D.R. Mullineaux, eds., *The 1980 Eruptions of Mount St. Helens, Washington*, U.S. Geological Survey Prof. Paper 1250 (U.S. Gov't. P.O., Washington, 1981).

36. J.G. Moore and W.C. Albee, in Ref. 35.

37. S.W. Kieffer, pp. 379-400 in Ref. 35.

38. See, for example, M. Malin and M. Sheridan, Science **217**, 637-640, 1982; J. Eichelberger and D. Hayes, J. Geophys. Res. **87**, 7727-7738; or J. Moore and C. Rice, in *Explosive Volcanism: Inception, Evolution, and Hazards*, edited by F.M. Boyd (Nat. Acad. Press, Washington, 1984), Chap. 10.

39. JANNAF [Joint Army, Navy, NASA, Air Force] Handbook of rocket exhaust plume technology, Chemical Propulsion Information Agency Publication 263, Chap. 2 (1975).

40. S.W. Kieffer and B. Sturtevant, J. Geophys. Res. **89**, 8253-8268 (1984).

41. S.W. Kieffer, in *Explosive Volcanism: Inception, Evolution, and Hazards*, edited by F.M. Boyd (Nat. Acad. Press, Washington, 1984), Chap. 11.

42. M.J. Davis and E.J. Graeber, EOS: Trans. Amer. Geophys. Union **61**, 1136 (1980).

43. S.W. Kieffer and B. Sturtevant, Erosional furrows formed during the lateral blast at Mount St. Helens, May 18, 1980, submitted to J. Geophys. Res.

44. Comprehensive reviews of this work can be found in L. Wilson and J.W. Head III, Nature **302**, 663-669 (1983), and in R.S.J. Sparks, Bull. Volcanol. **46** (4), 323 (1983).

45. Review articles on Ionian volcanism can be found in D. Morrison, *Satellites of Jupiter* (U. Arizona Press, Tucson, 1982), including S.W. Kieffer, Chap. 18; see also Ref. 41.